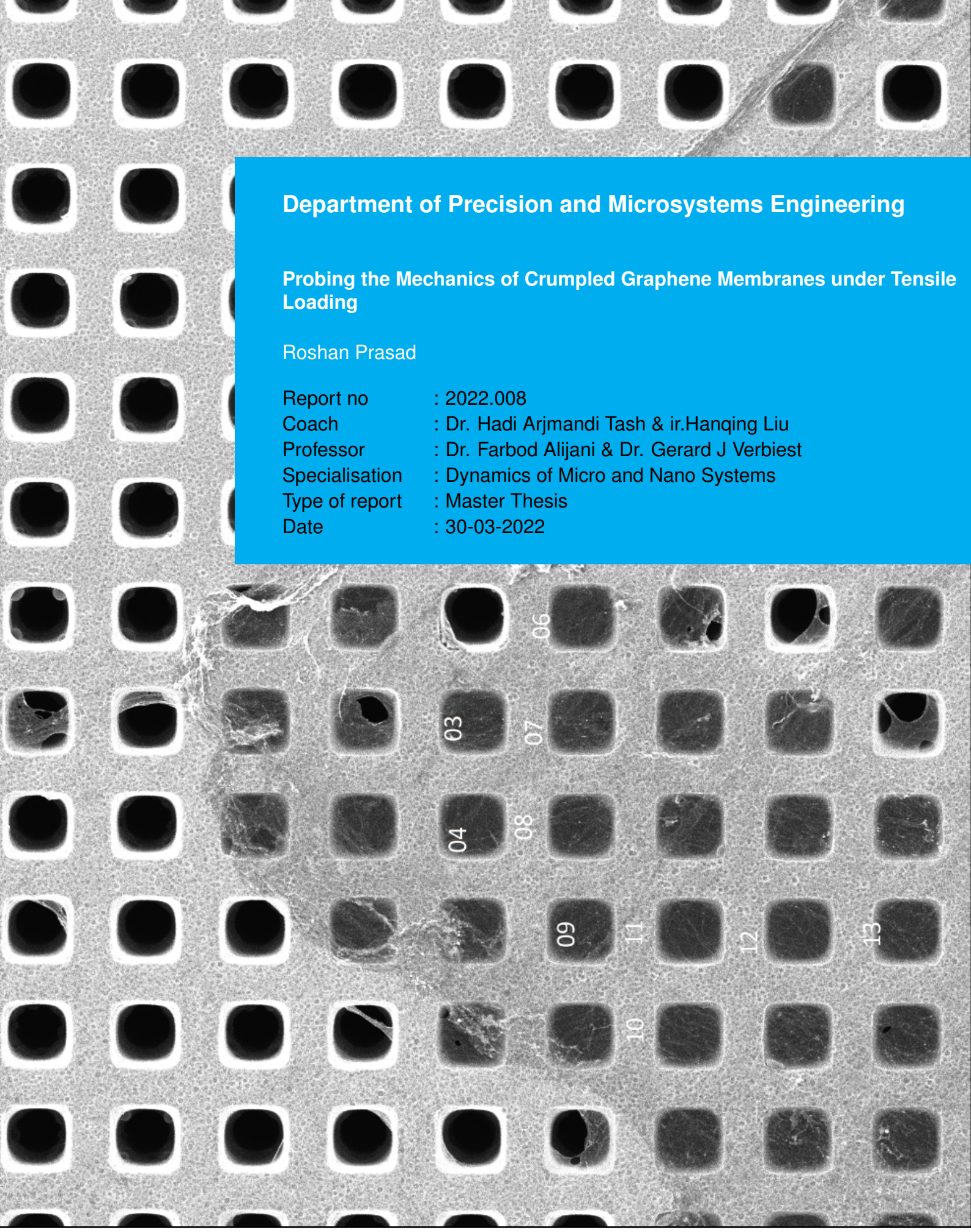

Department of Precision and Microsystems Engineering

Probing the Mechanics of Crumpled Graphene Membranes under Tensile Loading

Roshan Prasad

Report no	: 2022.008
Coach	: Dr. Hadi Arjmandi Tash & ir.Hanqing Liu
Professor	: Dr. Farbod Alijani & Dr. Gerard J Verbiest
Specialisation	: Dynamics of Micro and Nano Systems
Type of report	: Master Thesis
Date	: 30-03-2022

TU Delft Delft University of Technology

Challenge the future

Probing the Mechanics of Crumpled Graphene Membranes under Tensile Loading

An Experimental Study

by

Roshan Prasad

to obtain the degree of

MASTER OF SCIENCE
in Mechanical Engineering

at the Delft University of Technology,
to be defended publicly on Wednesday, March 30, 2022 at 14:45 hrs.

Student number :	5044685	
Project duration :	November, 2020 - March, 2022	
Thesis committee :	Dr. ir. F. Alijani,	TU Delft, Supervisor
	Dr. ir. G.J. Verbiest,	TU Delft, Supervisor
	Prof.dr.ir. A. van Keulen,	TU Delft, External
	Dr. ir. H. Arjmandi Tash,	TU Delft, Daily Supervisor
	ir. H. Liu,	TU Delft, Daily Supervisor

Faculty of Mechanical, Maritime and Materials Engineering (3mE) · Delft University of Technology

"Never let your head hang down. Never give up and sit down and grieve. Find another way. And don't pray when it rains if you don't pray when the sun shines."

-Leroy Satchel Paige

Acknowledgement

The road to the completion of the master thesis was not very straightforward. Many challenges needed to be surpassed, both personal and academic. However, the only belief that kept me going was that there is always something at the end of the tunnel. Through this thesis, I learned a lot, both academic and about life, and one such thing is not to underwhelm even the most minor contribution you have made.

At this juncture of my masters' education, I would like to thank the people who have been of great help and support throughout the journey. I am grateful to professors Farbod and Gerard for providing me with this opportunity to work in the Dynamics of Micro and Nano Systems group. I would also like to thank Hadi and Curry for putting up with me throughout this journey. Above all, I need to thank the four of them for their continuous supervision and guidance. They provided me with valuable suggestions and knowledge, without which I wouldn't have been able to complete the master thesis. Apart from the academic point of view, they also supported me during my personal hardships.

I would like to thank Livia for her training on the JPK atomic force microscope, without which the research wouldn't have been possible. I would also like to thank Ali for his insights into graphene study, which helped me understand the work better and obtain better results. I would like to express my gratitude to Rob for his technical support throughout the thesis period.

I will forever be thankful to my parents and friends, who are my support pillars, without whom I would not be in this position. I would like to use this chance to thank all my lecturers and professor for their guidance and knowledge, which triggered my interest in the field of science. Thank you, everyone, for everything!

Roshan Prasad
March 25, 2022

Abstract

Graphene is considered a promising material due to its unique electrical characteristics and excellent mechanical properties. These extraordinary properties make graphene a suitable material for applications like mechanical reinforcements, protective coatings, supercapacitors, sensors, etc. However, when trying to extract these properties experimentally, the challenge of producing pristine graphene prohibits researchers from attaining the required results. The challenge is primarily due to the formation of structural or surface imperfections during the fabrication, transfer or manipulation of the membrane. In addition, graphene possesses a low bending rigidity which inevitably leads to the out-of-plane crumpling of the film. So, determining the effect of these imperfections on the mechanics of graphene is critical to ensure development in the research field and application pertaining to graphene. The main focal point of this work is to experimentally determine the effects of surface corrugations, in the form of out-of-plane crumples, on the mechanical constants of the graphene membrane. In this study, two types of graphene membranes are considered, one is a flat membrane, and the other is a heavily crumpled membrane. The atomic force microscope is used to probe the membranes, and the mechanical constants are extracted from the resulting force-deflection characteristics. The mechanical constants of the flat membrane, 2D Young's modulus (E_{2D}) and pretension (σ_0) were found to be 140.42 ± 44.52 N/m and 0.119 ± 0.049 N/m respectively. The values obtained suggest a softening behaviour of the membranes, which is due to the intrinsic crumpling of the membrane in the out-of-plane direction. Surprisingly, in the case of heavily crumpled membranes, E_{2D} and σ_0 were found to be 393.34 ± 145.12 N/m and 0.203 ± 0.069 N/m respectively. The values obtained suggests that the heavily crumpled membranes provide greater resistance to deflection than the flat samples. However, it is essential to understand that the values do not depict the effective Young's modulus or intrinsic strength of the membrane. The presence of folds in the heavily crumpled membranes is the reason for their higher resistance to deflection. The evolution of these folds, when subjected to nanoindentation, is also discussed in this work. This research helps provide insights into how the graphene membrane responds mechanically in the presence of crumples and also provides progress in realising the applications of crumpled graphene membranes.

Contents

1

Introduction

Graphene, a one-atom-thick film, was first isolated in 2004 by Andre Geim and Konstantin Novoselov [1]. Since then, the investigation into the properties and applications of the graphene membrane has been fast-growing. Over the years, researchers have found graphene to possess exceptional mechanical, optical, electrical and chemical properties. For example, graphene is considered to be the strongest material measured (Young's modulus = 1 TPa)[2]. These properties pave the way for possible applications in a large number of fields. However, before the possible applications can be fully realised, it is essential to understand the properties of graphene thoroughly. Researchers, over the years, have tried to understand the properties of the material experimentally. However, in most cases, the full potential of graphene was not understood due to the presence of imperfections in the sample. These imperfections are either structural defects or surface corrugations developed during the fabrication or processing of the graphene samples. The structure and topography of the material play an immense role in the mechanical aspects of the material. This makes the development of these imperfections and their effects on the mechanical properties of graphene a vital avenue in the field of research. Recent theoretical studies have shown that these imperfections have a significant effect on the mechanical response of the graphene samples[3, 4]. However, the experimental validation of some of these theoretical results, mainly surface corrugations, are still unexplored. In addition to this gap in research, researchers have shown that graphene with surface corrugations also possess some exciting applications like energy storage and strain sensing [3]. So, to bridge this research gap and possibly realise the applications of graphene with surface corrugations, it is necessary to study the effect of surface corrugations on the mechanical response of the monolayer graphene membranes experimentally.

This research aims to experimentally determine the effect of crumpling (surface corrugation) on the mechanics of the graphene membrane. The research done is structured in the following manner. The first chapter deals with the introduction and motivation for this research. In the following chapter, which is the literature review, the introduction to graphene, the possible structural and surface imperfections, and its current state of research is provided. In addition, the chapter also deals with the different fabrication, transfer and measurement techniques used by researchers to investigate the properties of the graphene membrane. Chapter 3 deals with the research gap present and the objectives of this research. In chapter 4, the methodology followed during the research is presented. The next chapter presents all the findings of this research and its understandings. The final part of the report deals with the conclusions that can be drawn from the findings and the possible recommendations that can be given for future research.

2

Literature Review

This chapter aims to provide a basic understanding of graphene and its properties. In addition, the current state of research regarding the possible imperfections and their effects on graphene mechanics are also discussed. This chapter also provides a brief review of the different fabrication, transfer and mechanical testing methods of graphene membranes, from which the desirable choices can be made for this work.

2.1. Introduction to Graphene

Graphene is a two-dimensional membrane that consists of only carbon atoms. It is one-atom-thick and is considered the structural element of many carbon-based structures. In graphene, the carbon atoms are organised in a honeycomb structure, forming a tightly packed hexagonal crystal lattice, which is bonded by strong covalent bonds, as shown in fig 2.1. These covalent bonds are sp^2 hybridised, which means that a single carbon atom is attached to each of the neighbouring three carbon atoms by one σ-bond, and the fourth bond is a π-bond which is oriented out-of-plane. These membranes are commonly known as pristine graphene if the structural integrity of the membrane is maintained without any impurities or defects.

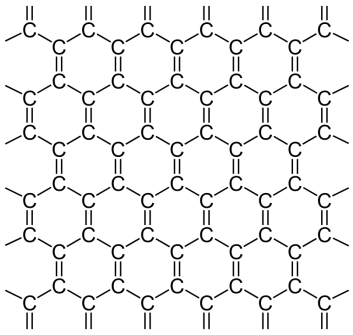

Figure 2.1: Hexagonal lattice structure of graphene

Production of pristine graphene was a significant challenge until the rise of high-quality methods like Chemical Vapor Deposition (CVD) and mechanical exfoliation. The major drawback of these methods is the scalability of the process. Some scalable methods exist, but they produce low yields and are expensive for mass production or industrial use.

2.1.1. Properties of Graphene

Various researchers have been keen to understand and quantify the reportedly exceptional properties of graphene. The structure of the graphene membrane places a vital role in understanding its properties. Some of the reported properties of the membrane is a work of simulation, and the experimental validation of these results are yet to be obtained. The different properties of graphene are discussed below.

Electrical Properties

The charge carrying capability and electron mobility are important properties pertaining to the electrical properties of graphene. Kim et al.[5] were able to show that CVD grown graphene which were transferred onto SiO_2 substrate possessed an electron mobility of $\mu = 3700 cm^2/(V.s)$ at electron densities of $n = 5 \text{ x } 10^{12} cm^{-2}$. Whereas K.I. Bolotin et al.[6] showed that for suspended graphene the electron mobility can rise up to $\mu = 2 \text{ x } 10^5 cm^2/(V.s)$ at electron densities of $n = 2 \text{ x } 10^{11}\ cm^{-2}$. The conductivity of graphene, dependent on the electron mobility and charge density, is affected by the low charge density. Zhao et al.[7] showed that this could be tackled with the help of nitrogen dopant, as the electronic structure of graphene only changed within a few lattice spacing while increasing the carrier density. These properties of graphene attribute to the type of hybridisation, as the free π bond in the sp^2-hybridisation, is responsible for the electronic conduction.

Optical Properties

The optical transmittance and reflectance of graphene are some of the main parameters of study to understand the optical behaviour of graphene membranes. R.R.Nair et al.[8] observed the reflectance to be negligible (<0.1%) and also showed that the opacity could reach ~ 2.3% which in turn implies that the transmittance of ~ 97.7% can also be reached for a single layer graphene membrane. They also showed that the opacity could be increased by 2.3% by adding a graphene layer.

Thermal Properties

Researchers have studied the thermal conductivity and the thermal expansion coefficient of graphene to a great extent. Balandin et al.[9] used the Raman spectroscopy to determine the thermal conductivity (κ) of suspended graphene, and he had reported very high thermal conductivity values up to $\kappa \approx 5000 \text{ Wm}^{-1}\text{K}^{-1}$. They further reasoned it out to be due to the lattice vibrations created by the free dangling bonds, which in turn is responsible for efficient heat transfer[10].
At low temperatures, graphene possesses a negative thermal expansion coefficient, owing to the dynamic rippling present in the membrane [11]. However, Gao et al.[12] later reported that at higher temperatures, graphene's thermal expansion coefficient becomes positive. They also showed that the anharmonic interactions suppress the dynamic ripples. This transition in the thermal expansion coefficient is still an important research topic as the transition temperatures are still inconsistent.

Mechanical Properties

The stability of the sp^2 bonds is the main reason behind the exceptional mechanical properties of graphene. Graphene may deform by in-plane stretching or out-of-plane bending, making the in-plane and bending moduli the most important elastic properties. Lee et al.[2] were the first to experimentally report the mechanical properties of suspended graphene by nanoindentation, using an Atomic force microscope (AFM). The force-displacement behaviour as depicted in fig 2.2 was understood to be due to the nonlinear elastic properties of graphene membranes. The authors obtained a value of 340 ± 50 N/m for graphene's second-order elastic stiffness (2D Young's modulus). Assuming a nominal thickness of 0.335 nm, the 3D Young's modulus of the graphene membrane was found to be 1.0 ± 0.1 TPa. The analytical model used in the article is still a debatable topic. The model obtained by summing up two asymptotes seems to be providing more errors than the simu-

lation results[13]. Using the same experimental setup, Lee et al. also measured the intrinsic strength of single-layer graphene. The breaking strength was found to be ≈ 42 N/m, which corresponds to an intrinsic strength of 130 GPa.

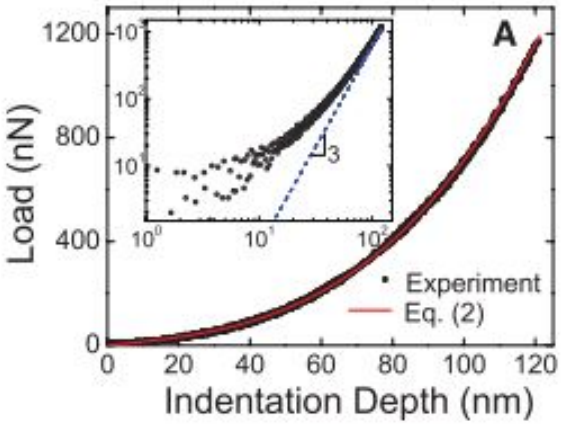

Figure 2.2: Force-displacement data of suspended graphene using AFM nanoindentation[2]

In order to extract the in-plane elastic properties using the AFM, the effect of the bending modulus of graphene is considered to be negligible; this is justified as a membrane-like behaviour. However, the direct measurement of the bending modulus of graphene or any 2D material is quite challenging. The bending modulus of single-layer graphene was found to be ≈ 1.2 eV, which was obtained from the phonon spectrum of bulk graphite[14]. Lindahl et al.[15] later obtained the bending modulus of ≈7.1 eV, based on the measurements of the critical voltage of pre-buckled graphene sheets. This value has a lot more uncertainties associated with it due to limited data points obtained. In the recent past, Blees et al.[16] inferred the bending modulus from the spring constant of a graphene cantilever structure using an elementary mechanics model. This method surprisingly yielded values around 10^3-10^4 eV, which was attributed to the effect of static and thermal ripples. Looking at the articles, there still exists a large discrepancy in the theoretical and experimental values of the bending modulus of graphene, which calls for further research.
Fracture toughness is also one of the critical properties related to engineering applications. Zhang et al.[17] determined the fracture toughness of CVD graphene with the help of an in situ micromechanical testing device within a Scanning Electron Microscope (SEM). It can be understood from the results that the fracture toughness is dependent on the weakest region of the membrane. The authors initiated the brittle fracture of graphene by introducing a central crack using a Focused Ion Beam (FIB). They obtained the fracture toughness, which was measured as the critical stress intensity factor of K_c= 4.0±0.6 MPa.

The basic understanding of the properties of the graphene membrane shows that the exceptional properties can be used in various applications. However, a widespread in the theoretical and experimental values of some of the properties still exist. Furthermore, research also shows that these properties are altered due to changes in the lattice structure that are generally induced due to defects or other corrugations. These ambiguities and external influence show why the field of research about graphene still has many research gaps present. The following section deals with the common defects and corrugations developed during graphene's growth or transfer

2.2. Imperfections in Graphene

This section discusses the possible imperfections that can be induced into the lattice structure or the possible corrugations present in the membrane. Furthermore, the effects of these defects on the properties of the graphene membrane are also mentioned. It is well known that obtaining pristine graphene without any imperfections is a massive challenge on its own, which makes the study of these imperfections a critical research field. The types of structural and surface imperfections are as follows.

2.2.1. Structural Defects

Structural defects are the type of defects wherein the lattice structure of the membrane is altered by lattice reconstruction or atom displacement. These defects occur during the production process of graphene or the transfer process. A large number of structural defects may occur, but only the most common ones are discussed here and are as follows.

2.2.1.1. Point Defect

Point defects are zero-dimensional defects that occur at a single lattice point. When the lattice is disordered without the presence of a foreign atom, they are known as intrinsic defects. In contrast, in the presence of a foreign atom, they are referred to as impurities or extrinsic defects.

Stone-Wales Defect

Stone-Wales(SW) defect is an intrinsic defect wherein the crystal lattice of graphene reconstructs itself to form non-hexagonal rings. One of the C-C bonds rotates by 90°, transforming four hexagons into two pentagons and two heptagons[18]. J. Meyer et al.[19] were able to experimental obtain the Transmission Electron Microscope(TEM) image of the defect, as shown in fig 2.3(a.).

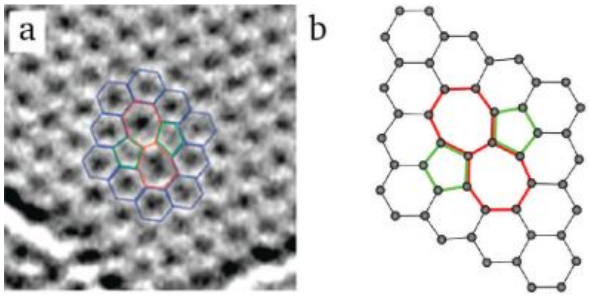

Figure 2.3: SW defect a.) Experimental TEM image[19], b.) Atomic structure obtained by DFT calculations[4]

Researchers, with the help of Molecular Dynamics(MD) simulations, have shown that SW defects have a small effect on the Young's modulus. In contrast, the failure strain and the intrinsic strength of the graphene decreased significantly in the presence of SW defects[20][21].

Vacancy Defect

Vacancy is a type of lattice defect in which the carbon atoms in the lattice are removed, which leads to the formation of voids. Graphene's unique ability of lattice reconstruction counteracts these vacancies by forming non-hexagonal rings. Irradiation of the graphene membrane with electrons or ions give rise to vacancies, and the energy of these electrons should be above the displacement threshold energy of carbon in the graphene lattice in order to remove the carbon atom[4].

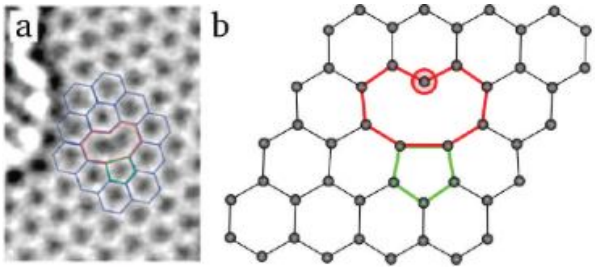

Figure 2.4: Single Vacancy defect a.) Experimental TEM image[19], b.) Atomic structure obtained by DFT calculations[4]

Vacancy type defect affects the mechanical properties of the graphene, where the effective Young's modulus decreases drastically with the increase in the defect density. This behaviour was reported using MD simulations by Tapia et al.[22]. Furthermore, they showed that the shear modulus followed a similar trend to the young's modulus. On the other hand, Wang et al.[20] reported that the vacancies decrease the fracture strength of the graphene membranes as well.

Contradicting to the above mentioned behaviour of defective graphene, Lopez-Polin et al.[23] experimentally showed that the in-plane Young's modulus of graphene increases with the increase in the defect density up to ~0.2%, after which the Young's modulus starts to decrease drastically.

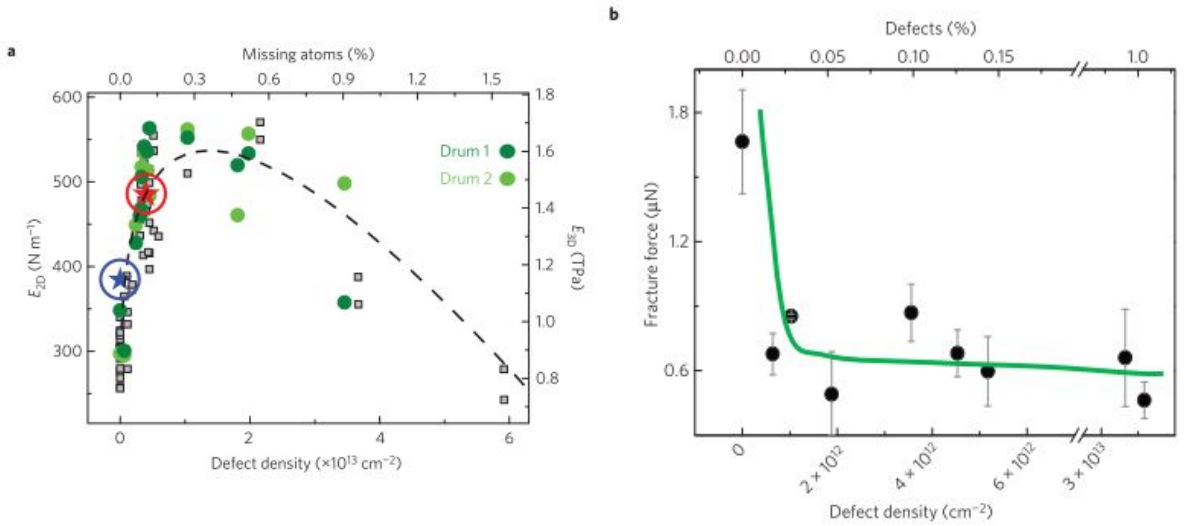

Figure 2.5: a.) E_{2D} as a function of the defect densities for two drumheads, b.) Fracture force as a function of the defect densities with error bars that correspond to the standard deviation.[23]

The authors attributed this behaviour to the suppression of the out-of-plane flexural modes due to the anharmonic coupling of the in-plane and out-of-plane fluctuations. The variation of the Young's modulus to the defect density is depicted in fig 2.5a. The authors also studied the fracture force of the membrane. Compared to the Young's modulus, a completely different behaviour was observed. The fracture force showed a rapid decrease with the increase in the defect density, after which a saturating tendency was observed at higher defect densities as shown in fig 2.5b.

Adatoms

Adatoms are atoms that are externally absorbed on the lattice structure of the graphene membrane. The lattice then re-configures to form a bridge, dumbbell or other configurations, as shown in fig 2.6. Different types of atoms can be absorbed onto the lattice, which makes the properties of the

graphene sheet heavily dependent on the type of atom absorbed. Banhart et al.[4] showed the impact of a carbon adatom on the lattice of the graphene membrane. The extra carbon atom's presence changed the bond's hybridisation from sp^2 to sp^3-hybridisation, which in turn reduces the in-plane stiffness of the membrane.

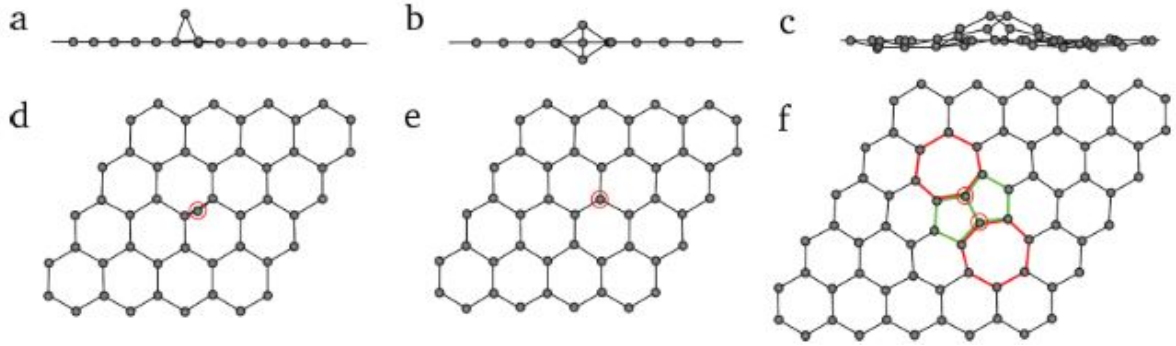

Figure 2.6: Adatom defect configurations: (a,d) single adatom in bridge configuration; (b,e) single adatom in dumbbell configuration; (c,f) two close adatom forming the 7557 configuration.[4]

Substitutional Impurities

Substitutional impurities are a type of defect in which foreign atoms replace the carbon atoms in the graphene lattice. Similar to adatoms, the change in the graphene membrane properties depends on the incorporated foreign atom. The bond length between the foreign atom and the carbon atom is different from that of the carbon-carbon bond, which makes the foreign atom to be located slightly off the graphene layer as shown in fig 2.7[4].

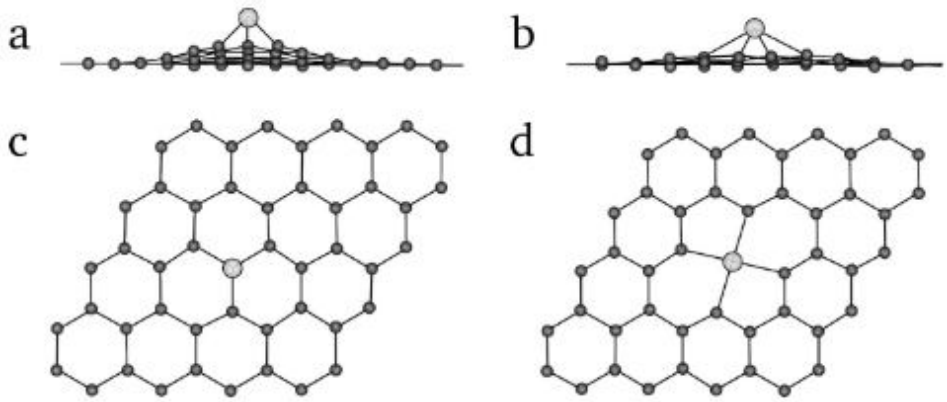

Figure 2.7: Substitutional Impurities defect configurations: (a,c) single vacancy in bridge configuration; (b,d) double vacancy; in both the images the small dark circles denote carbon and the large lighter circle denotes transition metals.[4]

2.2.1.2. One-Dimensional Defects

One-Dimensional defects, also known as dislocations, are an extension of point defects wherein the point defect is present at multiple lattice points. In other words, they can be visualised as a line of reconfigured point defects as shown in fig 2.8(a,b)[24]. These line defects may occur during the growth of graphene by CVD when there is a misfit between the metal substrate and graphene. This misfit leads to different grains having different orientations, and when grains with two different orientations coalesce, they lead to line defects. J.Lahiri et al.[25] showed the appearance of a line defect due to the mismatch between graphene and the Ni substrate, and this can be seen in fig 2.8c.

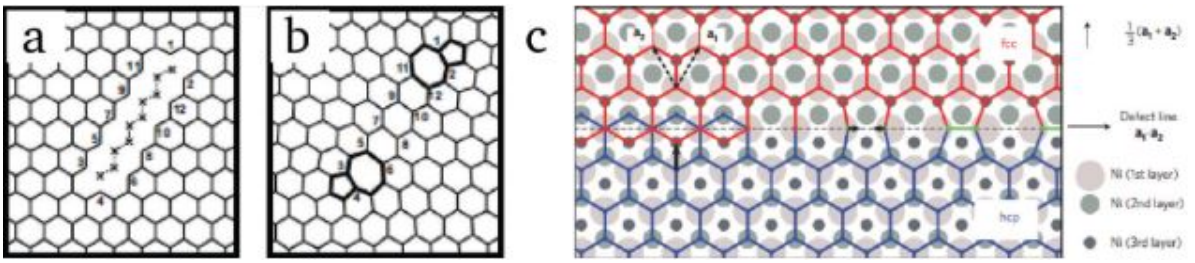

Figure 2.8: (a,b) Line defect formation along the multiple vacancy structures[24] c.) Grain boundary when graphene grown on Ni substrate [25]

2.2.2. Surface Corrugation

Surface corrugation can be understood as the out-of-plane deformation of the surface. These types of corrugation may occur during the growth, transfer or manipulation of graphene membranes. They can also be induced by introducing structural defects like grain boundaries into the lattice. The commonly observed surface corrugations are dynamic ripples, crumples and static wrinkles. In this section, an understanding of the three corrugations are discussed along with their impact on the mechanical properties of graphene.

2.2.2.1. Ripples

Membranes that are truly 2D are thermodynamically unstable, and the formation of ripples achieves this stability. Ripples are formed from the partial decoupling of the stretching and bending modes[26]. P.Xu et al.[27] used the Scanning Tunneling Microscope(STM) to understand the formation of ripples and found that the ripples are dynamic in nature. Furthermore, they found that the asymmetry in the bond lengths due to the delocalized π electrons forces the carbon atom in the lattice to move into the third dimension to reduce the free energy. It is well known that the large scale production of graphene by CVD induces defects. Seung and Nelson[28] showed that corrugations or out-of-plane deformations help in the reduction of in-plane stresses induced by these defects. Therefore, induced defects like the dislocations or grain boundaries can lead to the formation of ripples to reduce the in-plane stresses.
Multiple simulation studies have been performed to understand the effect of ripples on the mechanical properties of the graphene membrane. Ripples tend to produce a nonlinear stress-strain behaviour even at small strains, and it was also noted that the amplitude of the ripples decreases rapidly with the increase in the strain of the membrane[29][30]. Apart from this, the temperature has a significant effect on the ripples, which affects the mechanical properties of graphene. Lee et al.[30] observed that the out-of-plane displacements increased with an increase in the temperature, and this, in turn, leads to a near-linear decrease of the elasticity of the membrane. Furthermore, temperature also affects the Poisson's ratio as well as the thermal expansion coefficient of the membrane. Zakharchenko et al.[31] were able to see a transition in the sign of the Poisson's ratio at around 1700k, where the Poisson's ratio changed from positive to negative.

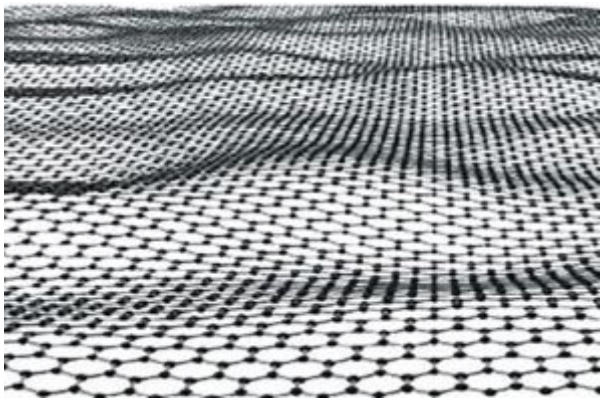

Figure 2.9: Rippled graphene[3]

A similar transition was also noticed in the thermal expansion coefficient of graphene, where Gao et al.[29] found that graphene has a negative thermal expansion coefficient at low temperatures and a positive thermal expansion coefficient at high temperatures. The authors cited that this was because the out-of-plane vibrations were energetically preferred over the in-plane vibrations.

2.2.2.2. Crumples

Crumples are out-of-plane deformations of the graphene membrane, which may alter the geometry depending on the distribution of stress across the surface of the membrane as seen in fig 2.10(a,b). Since crumpling is heavily dependent on stress distribution, the properties of crumpled graphene may be affected in different ways.

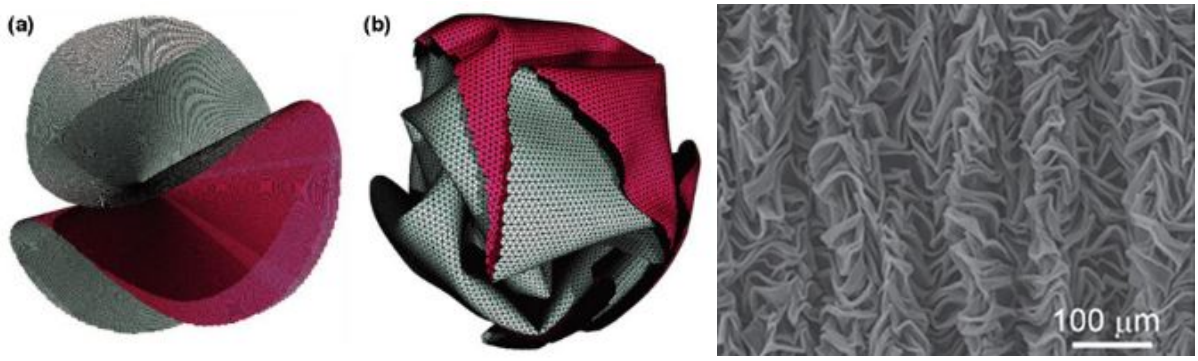

Figure 2.10: Mechanical model of crumpled sheet:a.)applying weak force b.) applying strong force; c.) SEM image of crumpled graphene.[3]

Nicholl et al.[32] stated that the crumpling is predominantly due to the static wrinkles caused by the uneven stress distribution and the out-of-plane flexural phonons. They investigated the influence of these two mechanisms on the in-plane stiffness of the membrane and found that the in-plane stiffness of the crumpled graphene had reduced to 20-100 N/m. Furthermore, the authors suppressed the effect of static wrinkles by cutting into graphene ribbons and found that the in-plane stiffness increased from 36 to 300 N/m. The authors inferred that the softening of the membrane is predominantly due to the static wrinkles with minor contributions from the flexural phonons.

2.2.2.3. Wrinkles

Wrinkles are a type of corrugation caused by the membrane's local buckling. Wrinkles can be induced by different mechanisms, which in turn gives rise to different wrinkling patterns.

Graphene growth on a metal substrate is one of the main ways wrinkles are generated. Graphene sheets having a negative thermal expansion coefficient (TEC) at low temperatures due to reduced flexural phonon modes tend to expand during the cooling process. In contrast, the metal substrate shrinks during cooling due to its positive TEC, and this mismatch in the TEC results in the straining of the membrane, which in turn induces wrinkles into the membrane, as shown in fig2.11[33].

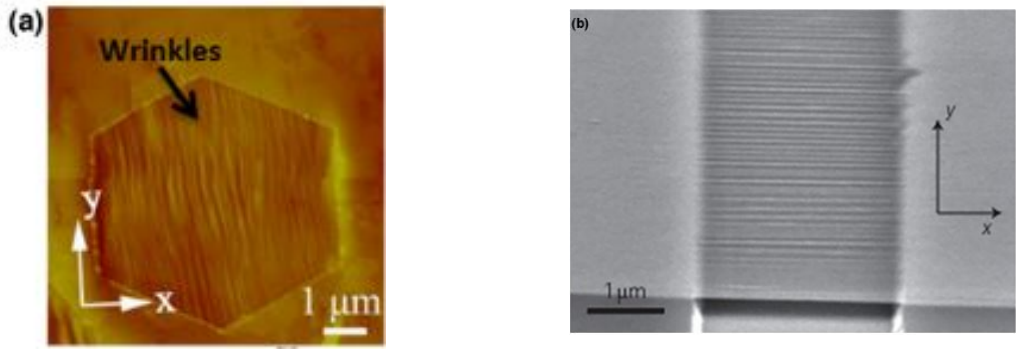

Figure 2.11: a.)AFM image of wrinkled graphene on Cu substrate b.) SEM image of wrinkled graphene[3]

Wrinkles are also formed during the wet transfer of graphene. After removing the polymer by dissolving it in a solvent, the membrane is transferred to the substrate present in the bottom of the liquid, during which wrinkles may form on or along the water drain channels present on the interface between the membrane and the substrate. Figure 2.12(a-g) gives a schematic view of the formation of wrinkles during the wet transfer of graphene. Furthermore, the orientation of the wrinkles can be controlled by altering the morphology of the substrate, as shown in fig 2.12(h). Altering the morphology may induce additional stress because of the adhesion between the graphene and substrate, which, in turn, may increase the number of wrinkles[34].

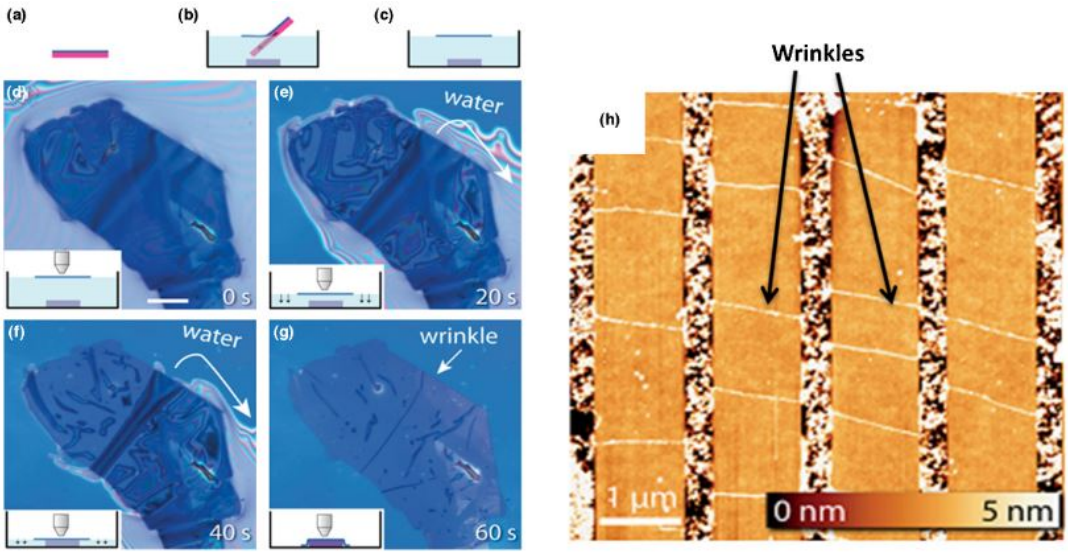

Figure 2.12: (a-c) Schematic view of transfer process, (d-g) Optical images of the formation of wrinkle;(h) AFM image of graphene transfer on a step structure.[34]

The fracture stress of wrinkled graphene membrane was studied by Min and Aluru[35] using molecular dynamics. They had performed a shear test to obtain the fracture stress and found the value to be around 60 GPa which is less than the 97.5 GPa obtained for a flat graphene membrane.

The results indicated the softening of the membrane due to the presence of wrinkles. On the other hand, Qin et al.[36] simulated results pertaining to the interlayer shear properties of multi-layer wrinkled graphene. They tuned the topological defects in the membrane to obtain different aspect ratios of the wrinkled sheet. By adjusting the aspect ratio, they obtained a shear modulus of 1100 MPa and a strength of 610 MPa for an aspect ratio of s = 0.177. These results are considerately higher than that of the multi-layer flat graphene, which is understood to be due to the geometrical interlocking of the wrinkled graphene layers.

The information provided in this section deals with the commonly possible imperfections in graphene membranes. Based on the content, it is pretty evident that imperfections considerably affect the mechanics of the graphene membrane. Theoretical and experimental studies have been conducted to study the effect of imperfections like vacancy defects and line defects. However, the experimental study related to the effects of static wrinkles and crumples on the mechanics of graphene is still an ongoing field of research. Theoretical studies have shown that static wrinkles or crumples degrade the membrane. However, an experimental backing would help explore various aspects beyond the mechanics of wrinkled graphene. So, to study the impact, it is necessary to produce controlled crumples to quantify or correlate between crumpling and the mechanical property.

2.3. Fabrication and Transfer of Graphene

The section below deals with a few commonly used methods of fabrication of graphene and also concentrates on the types of transfers that can be done for Chemical Vapour Deposition (CVD) graphene onto the desired substrate.

2.3.1. Fabrication of Graphene

The fabrication of graphene has been one of the most attractive research fields worldwide since graphene, in general, has outstanding properties and applications. However, some of the crucial factors that have hindered the research are the cleanliness, cost, scalability of the process, or the obtained graphene's homogeneity. A good number of fabrication techniques have been developed so far, considering the difficulties involved. These techniques can be distinguished into two categories: top-down and bottom-up. The Top-down approaches are basically the exfoliation or breakdown of graphite to form graphene. In comparison, the bottom-up approaches are the chemical interaction or reaction of molecules to form the two-dimensional network of carbon atoms. In order to understand both these categories better, different types of mechanical exfoliations and chemical vapour deposition are discussed below.

2.3.1.1. Mechanical Exfoliation

Mechanical exfoliation is one of the top-bottom approaches available, wherein mechanical force is used to break down graphite until graphene is obtained. In order to exfoliate graphite, it is necessary to overcome the van der Waals attraction force, which is present between the layers in bulk graphite. Generally, two different paths can be taken to overcome the attractive force, one if by applying the normal force and the other is by applying lateral or shear force as illustrated in Fig 2.13[37].

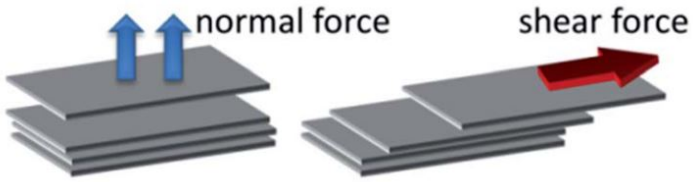

Figure 2.13: Types of mechanical paths to exfoliate graphene (normal and shear force)[37]

Micromechanical Cleavage

Micromechanical Cleavage is an approach wherein a normal force is applied to the bulk graphite to cleave it into thinner flakes. It can be said that the first-ever graphene flake was obtained by this method in 2004[1]. In this method, highly ordered pyrolytic graphite bulk is transferred to a scotch tape, and then the tape is stuck to itself. The tape is then ripped open, which is a form of normal force being applied to separate the layers. This adhesion and separation have to be repeated numerous times to obtain very thin flakes. The process is depicted in fig 2.14.

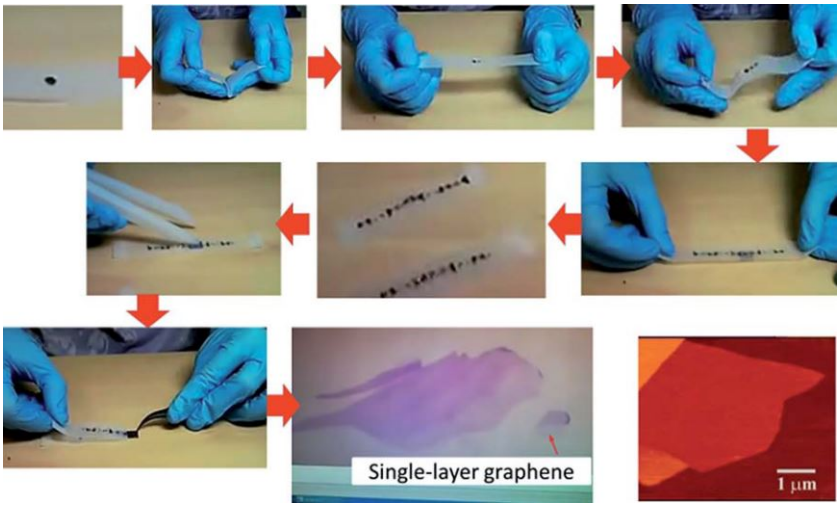

Figure 2.14: Step wise procedure of the scotch tape method to exfoliate graphene[1]

Over the years, large-area and high-quality graphene have been obtained using this method. In addition, most of the initial properties discovered for graphene were based on the flakes fabricated by this method. However, it is very time-consuming, labour intensive, and seems to be restricted to laboratory usage.

Three-roll Milling

Similar to the Scotch tape method, this process uses a three-roll mill machine and polyvinyl chloride (PVC) dissolved in dioctyl phthalate (DOP) as the adhesive[38]. The graphite flakes are made to run over the three-roll mill from the feed roll to the apron roll and then back to the feed roll as shown in fig2.15.

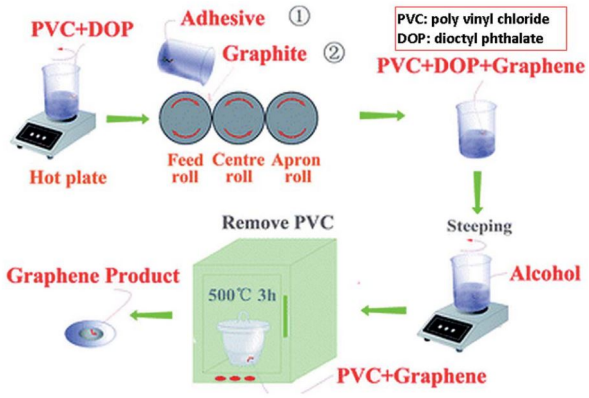

Figure 2.15: Depiction of the 3-roll milling process of graphite to obtain graphene[38]

The flakes are run continuously over the mill to obtain very thin flakes, up to single-layer graphene. The prepared adhesive is poured onto the three-roll mill while the graphite flakes are run over it. The graphite flakes disperse and then exfoliates in the adhesive. The issue of labour intensity and time consumption can be solved using this method, but the complete removal of the adhesive from the graphene flakes has its own issues.

Sonication

Exfoliation of graphite to obtain graphene on a larger scale has been done in the liquid phase with the assistance of sonication. The exfoliation of graphite through sonication can be better explained based on its mechanics. The liquid cavitations that are formed during the sonication are responsible for the exfoliation[37]. These cavitations induce bubbles in the liquid medium and these bubbles spread around the graphite. Shock waves or micro-jets are produced when the bubbles collapse, and these micro-jets start to impact the graphite surfaces, forming compressive stress waves throughout the graphite. As per the theory of stress waves, tensile stress waves are reflected onto the graphite when the compressive waves reach the free interface of graphite. The tensile stress generated from multiple collapses causes the graphite flakes to exfoliate. The micro-jets produced can also exfoliate graphite flakes by acting as wedges and splitting the layers by shear effect. The two methods are illustrated in fig 2.16.

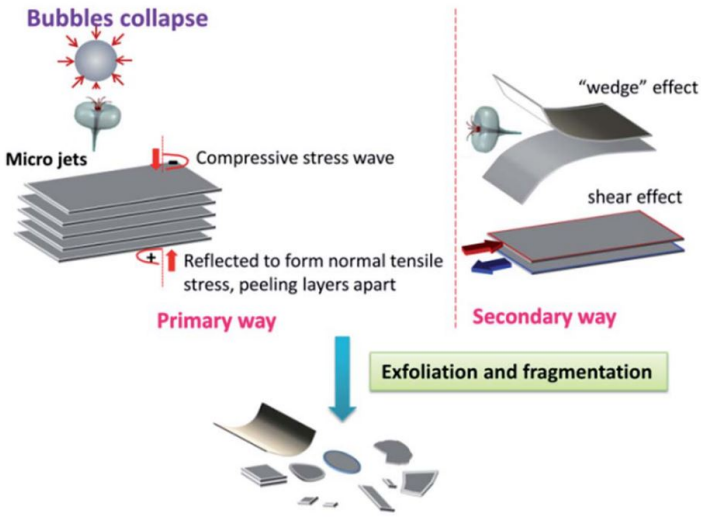

Figure 2.16: Depiction of the mechanism behind the exfoliation by sonication of the graphite[37]

Coleman et al.[39] obtained graphene by dispersing graphite powder in organic solvents like N-methylpyrrolidone (NMP) and N,N-dimethylformamide (DMF), later sending the mixture through sonication and centrifugation. The method seemed easy, and the obtained graphene was of good quality. However, the method produced a very low concentration of graphene, approximately 0.01 mg/ml. Researchers have tried to increase the concentration of graphene by modifying the sonication time, mixing solvents, increasing the initial concentration of graphite and many others. However, many more variables are involved, which restrict the researchers from obtaining an optimum condition to achieve a high concentration and quality of graphene. Researchers have shown that the graphene obtained by sonication has many defects. Even though cavitations are required for the exfoliation of graphite, they are the primary reasons for these defects as it is a harsh process that generally produces high temperatures and pressures[40]. Nanzai et al.[41] showed that the intensity and the distribution of the cavitations are heavily reliant on the shape and size of the vessel in which the sonication takes place as localized cavitation might take place.

Ball Milling

Ball milling is a technique in which lateral or shear force is used to exfoliate graphite into graphene. In ball milling, there are two types of effects that the graphite flakes experience by which exfoliation or fragmentation occurs. The two effects are shear force, which is desired for obtaining high-quality large-area graphene and impact or collisions with the balls, which takes place during the rolling action[37]. The two effects are depicted in fig2.17. In order to obtain high-quality large-area graphene the effect of collision has to be minimized as it tends to covert the crystalline nature into powder or amorphous form.

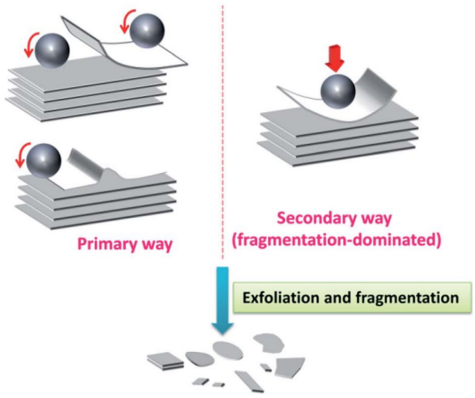

Figure 2.17: Depiction of the mechanism behind the exfoliation by Ball milling of graphite[37]

Ball milling is understood to be an excellent method for the large-scale production of graphene as they perform efficient exfoliation and can also be used to functionalize graphene. Nevertheless, the defects associated with the collisions involved during grinding is unclear. Basically, defects and fragmentation cannot be avoided since collisions cannot be avoided during the milling process.

2.3.1.2. Chemical Vapour Deposition

Chemical vapour deposition (CVD) is based on the bottom-up approach where molecules chemically interact to form sp^2 hybridised chain of carbon atoms. CVD is a process consisting of a chamber (quartz tube) connected to gas inlets and outlets. Inert gas (Ar) and transport gas (H_2) are fed into the chamber, maintained at a particular pressure and temperature. The chamber consists of a substrate, generally a transition metal onto which the carbon atoms are to be deposited to form graphene. Carbon molecules (preferably hydrocarbons) known as the precursor can be fed

into the chamber from an external source or directly placed inside the chamber based on the phase of the precursor. Generally, gaseous precursors are fed from an external source, and in the case of solid or liquid precursors, it is directly placed inside the chamber. The schematic images of the two methods are shown in fig 2.18.

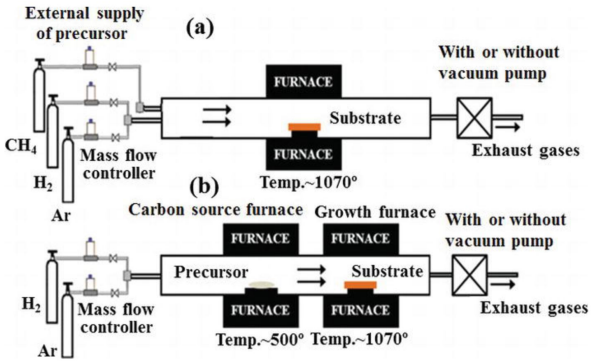

Figure 2.18: Schematic illustration of CVD process depending on the phase of the precursor used.[42]

The entire process of fabrication can be split into sub-steps which are as follows, precursor decomposition, dehydrogenation, diffusion of active carbon onto the transition metal or substrate, nuclei formation or nucleation and desorption[42]. Primarily, the substrate and chamber are heated to a specific temperature, and the precursor is thermally decomposed, leading to the formation of active carbon species. The thermal decomposition generally takes place close to the substrate to avoid the formation of carbon clusters. These active carbon species are absorbed onto the metal catalyst surface, after which the absorbed carbon atoms migrate on the surface of the substrate for nucleation and formation of films. The by-products of the carbon species are desorbed from the surface and then diffuse into the gas stream. The desorbed atoms from the substrate and the decomposed hydrogen are continuously pushed out of the chamber via the outlets. Each step in the entire process is heavily dependent on the variables or parameters involved in the process like temperature, pressure, gas flow rate, catalyst (type/size/shape), precursor and defects/vacancies on the catalyst surface. Understanding the effects of these parameters on graphene growth is vital in obtaining a high-quality graphene film. Researchers have studied the effect of these parameters separately[43] and have made significant progress towards optimizing the parameters for high-quality production. Over the years, it has been shown that CVD can produce high-quality graphene films with a minimum number of defects and that the resultant film can be used for various applications. However, the macro-level scaling of the production is, as of now, not possible due to the difficulties in the transfer of graphene, optimization of parameters and cost of production. Since the purpose at this point in the thesis is at a laboratory level, it is optimum to use CVD graphene because of its high quality and availability.

2.3.2. Transfer of CVD Graphene

Transfer of graphene has been an essential topic of research since graphene was obtained by scotch tape exfoliation. Even though CVD graphene grown on metal substrates are of high quality, the film experiences contamination and damages during the transfer process, which makes the need for high-quality transfer. The section below deals with the advancements in the transfer of CVD graphene to obtain clean and defect-free graphene films. In a larger view, the transfer techniques can be segregated as etching transfer and etching-free transfer, and these techniques are as follows.

2.3.2.1. Etching Transfer

A basic etching transfer involves the deposition/formation of a supporting layer which is primarily used to protect the film during the subsequent steps, etching the metal substrate on which the film was deposited during CVD, transferring the film along with the support to the target substrate and then removing the supporting layer[44]. The entire process of etching transfer is set to be time-consuming and complicated as each step needs immense care, and in the case of a slight mishap, the film suffers from structural damage or residuals. Over the years, thin Poly(methyl methacrylate) (PMMA) has been used as the supporting layer due to its flexibility, sufficient strength, insolubility in water, stability during etching and the ease of removal[45]. However, structural damages like cracks and tears have been reported while using PMMA. These damages have been reported to be due to the topography mismatch between the graphene membrane and the PMMA support layer caused by the trapped liquid medium between the two surfaces[46]. In order to remove the liquid medium, methods were adopted like usage of hydrophilic target substrates along with post treatment[47] and replacing water with volatile liquids like heptane, which readily spreads uniformly due to its low surface tension[48]. These adaptations have largely helped in the mitigation of structural damages.

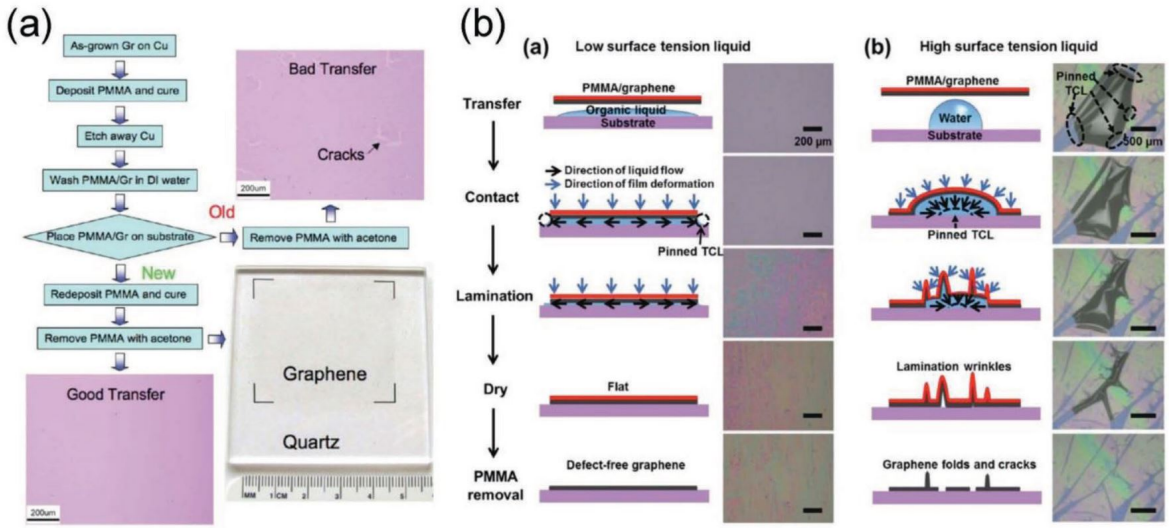

Figure 2.19: a) Etching transfer techniques of graphene with and without the redissolution of a PMMA layer.[46] b) Comparison between the transfer process of PMMA with graphene film using heptane(low surface tension) or water(high surface tension).[48]

On the other hand, these methods do not necessarily provide a clean transfer of graphene, which, in turn, degrades the electrical characteristics of the graphene film. Two broad techniques have been adapted to deal with the issue of clean transfer,i.e., usage of highly removable/dissolvable support and transfer without the usage of supporting layers. In the case of no supporting polymer layers, the target substrate is sometimes used as the support, wherein the contact between the target substrate and the graphene film is improved[49]. Later, in 2016, a method was developed wherein surface modification was used to facilitate the wafer-scale transfer of graphene membranes[50]. The technique uses a hydrophobic monolayer deposited on the SiO_2/Si substrate to increase the contact and mitigate the accumulation of liquid layers. This method is illustrated in fig 2.20. However, these methods are limited by the target substrate as specific substrates need to be used to obtain proper contact between the graphene film and the substrate. The usage of support-free methods can surpass the issue of contact. Even so, these support-free methods have their own drawbacks as graphene gets torn apart due to the high surface tension of the etchant solution[51] and is feasible

only for small size graphene.

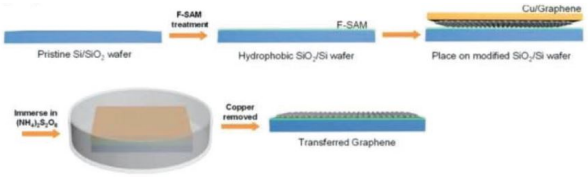

Figure 2.20: Transfer method in which the SiO_2/Si wafer is surface modified with a hydrophobic layer[50]

Alternatively, the technique of highly removable supports uses low-residue supports or improved post-treatments to remove the residuals. In the case of improved post-treatments, annealing in vacuum, enhanced rinsing with organic solvents, etching with radiolized water or thermal oxidation is used to remove the contaminants[52][44]. However, the residuals are not completely removed even after these post-treatments, which points towards the need for new polymers that are robust and as well as easily removable. The use of polystyrene, poly(bisphenol A carbonate), cellulose and rosin as the supporting layers proved to leave behind fewer residuals when compared to PMMA[53][44]. Although, using these supporting layers poses different problems like structural damages, small size or lower electrical performance.

2.3.2.2. Etching-free Transfer

The previous subsection discusses the chemical etching transfer of graphene. It can be understood that the method suffers from many drawbacks like contamination, heavy metal consumption, environmental pollution and incompatibility with noble metal substrates. Hence, etching free techniques are sometimes preferred for both clean and large-area transfer of graphene films. The etching-free techniques generally used to separate graphene from the metal foil are mechanical delamination, electrochemical intercalation and bubbling delamination[44]. However, the films obtained from these methods possess issues like low structural integrity and, in some cases, polymer contamination.

The technique of mechanical delamination is a dry etching-free transfer, wherein the interfacial interaction between the graphene film and the target substrate/support should be greater than the interaction between the graphene film and the metal foil for a successful transfer to take place. Researchers have used several strategies to improve the graphene-substrate interaction like the use of adhesives, in-situ polymerization, linker molecules or thermal deformation[44]. Using these approaches, intact mechanical transfer of graphene has been obtained. However, the graphene is affected by the roughness of the metal foil as the film tends to morph the topology of the foil[54]. Moreover, the challenge of large-area transfer and high structural integrity still exists due to the need for high control over the graphene growth as well as the delamination.

On the other hand, electrochemical bubbling transfer is an electrolysis method, wherein the graphene on metal foil along with the supporting layer is used as a cathode cell during the electrolysis process. The hydrogen bubbles generated during the water electrolysis are the reason for separating graphene from the metal foil. The graphene is later transferred onto the target substrate[55]. Studies show that the method is highly efficient, environmental friendly, versatile and comparatively lower in cost[56]. However, the method possesses a challenge of increasing the delamination rate without affecting the structural integrity of the graphene film.

Compared to the aforementioned etching transfer of graphene, the etching-free transfer is a bit more complex in terms of setups and the fact that the characteristics of graphene obtained from both methods are not significantly different. When weighing the complexity and cost of the experimental setup against the quality of the graphene film, we can say that the use of the basic etching transfer is more than enough to understand the effect of crumples in graphene. Moreover, by using etching transfer, the obtained results can be easily cross-referenced with previous works.

2.3.3. Controlled Production of Surface Corrugations

Surface corrugations play a considerable role in altering the properties of graphene, which makes the controlled manufacturing of them essential. Controlled fabrication also helps in the experimental investigation of the effects of these surface corrugations on the properties of the graphene sheets. Some of the methods used to produce these corrugations are mentioned below.
Taking advantage of the fact that graphene has a negative thermal expansion coefficient, Bao et al.[57] were able to produce controlled microscale wrinkles by thermal manipulation. Graphene membranes were transferred onto SiO_2/Si substrates that have predefined trenches, across which the membranes were suspended. Wrinkles were formed on the graphene membrane perpendicular to the trench direction (fig 2.21) when the membrane was annealed in a furnace. It is vital to note that these wrinkles heavily depend on the substrate's shape, structure, and temperature.

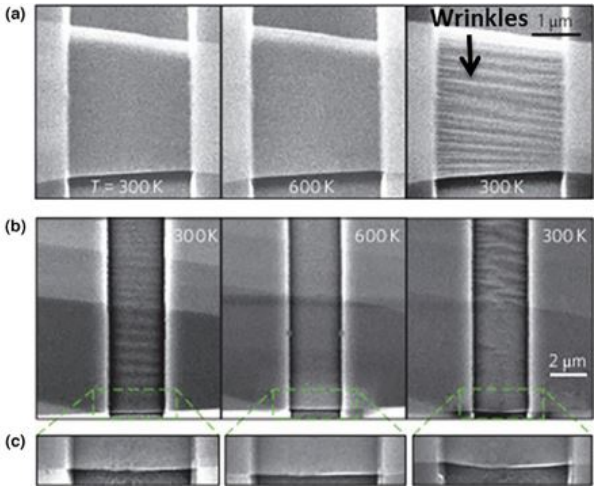

Figure 2.21: (a.) SEM images of graphene before, during and after the annealing process, (b.)SEM image of different trench, (c.) Magnified SEM image of the edges showing the slag of graphene into the trench after annealing.[57]

Wrinkles in graphene can also be produced by transferring the obtained pristine graphene onto a pre-stretched elastomer film. Zang et al.[58] proposed the same method wherein they biaxially stretch the acrylic-based elastomer and stamp the graphene over it. The elastomer was then relaxed in the pre-stretched direction one after the other. By relaxing one of the directions, they could obtain wrinkles parallel to the direction of relaxation. They further went on to obtain crumples by relaxing both directions. The amplitude and spacing of the wrinkles depended heavily on the pretension of the elastomer. Figure 2.22(a.) shows the schematic view of the relaxation of the pre-stretched elastomer, and figure 2.22(b.) shows the SEM image of the obtained wrinkles.

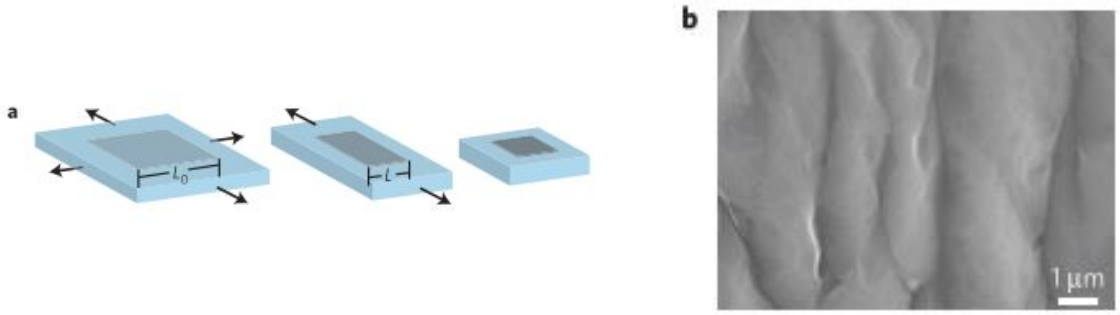

Figure 2.22: (a.) Schematic image of the relaxation of pre-stretched elastomer(b.) SEM image of wrinkled graphene[58]

On the other hand, Bai et al.[59] produced wrinkles by using thermal strain engineering, where CVD graphene was deposited on pre-trenched copper foils. The wrinkle positions were affected by the topography of the copper foils. The authors were successfully able to produce one-dimensional ripples of nano-scale size (2 nm to tens of nanometer) as shown in fig 2.23.

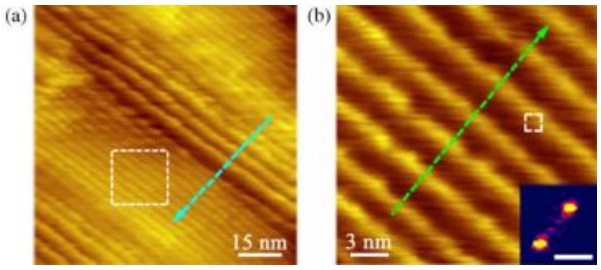

Figure 2.23: (a.) STM topography image of nanoscale ripples in graphene, (b.) Magnified STM image of white box.[59]

Another interesting method of controlled fabrication of wrinkles is the liquid phase shrink method[60]. In this method, the CVD grown graphene is suspended on the ethanol solution surface. The graphene membrane starts to self shrink, and the concentration of the ethanol solution can be altered to obtain uniformly distributed wrinkles at different heights. Chen et al.[60] showed that the so obtained wrinkled graphene has high stretchability, almost five times that of flat graphene. The schematic illustration of the wrinkling process is shown in figure 2.24(a).

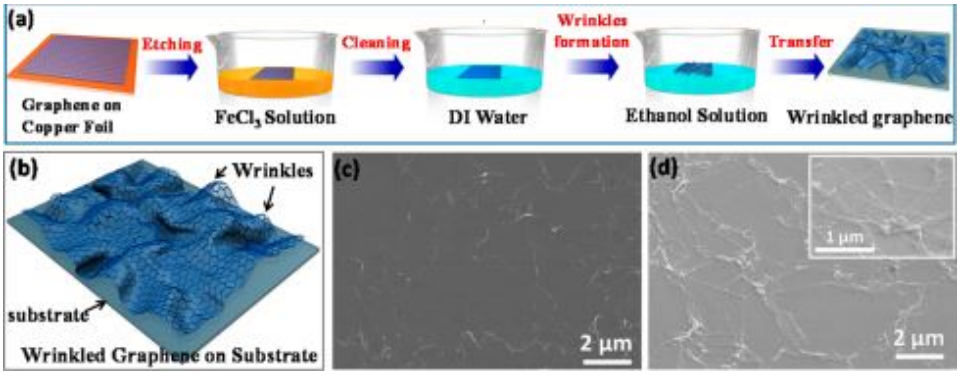

Figure 2.24: (a.) Schematic illustration of the liquid phase wrinkling method, (b.) Schematic image of the wrinkled graphene, SEM image of the graphene sample before (c.) and after (d.) liquid phase shrinking.[60]

Based on the available methods of obtaining graphene membrane with surface corrugation. The liquid phase shrinking method seems to be a simple and accessible method to produce out-of-

plane deformations. Having obtained the necessary membranes, the next would be to test these membranes. The following section deals with the commonly used testing methods to probe the mechanics of 2D membranes.

2.4. Mechanical Testing of Graphene

Mechanical characterisation of graphene is one of the most important research topics globally due to the need to understand the behaviour and properties of the graphene membrane. In this chapter, the different types of mechanical testing methods that can be used to probe the characteristics of graphene membranes are discussed.

2.4.1. Atomic Force Microscope (AFM)

AFM is a type of scanning probe microscopy wherein the information of a surface can be obtained with a resolution of up to a few nanometers. Researchers have used the AFM for force measurement, imaging and force manipulation. AFM is more preferred than some of the other scanning methods as it can provide both 2D and 3D images of the surface, and the images are produced with a pseudocolour to obtain high-resolution images. Apart from this, AFM can also be used to scan both conducting and insulating materials.

AFM nano-indentation was used to measure the Young's modulus, and the intrinsic strength of the graphene membrane by Lee et al.[2], wherein they suspended mechanically exfoliated graphene on Si substrate with circular patterned holes of diameter 1 and 1.5 μm. The authors obtained the force vs deflection curves for multiple suspended samples, which can be seen in figure 2.25(e.).

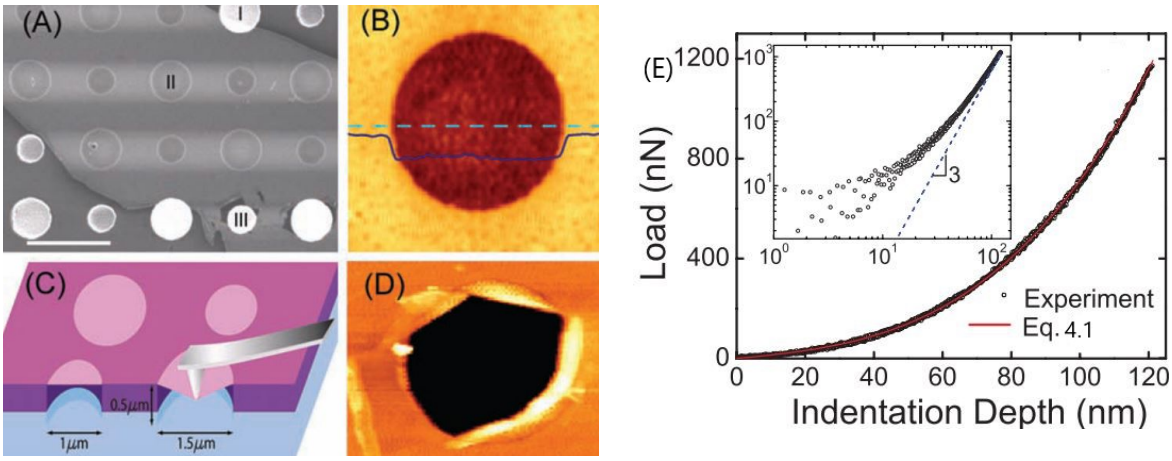

Figure 2.25: a.) SEM image showing the 2 different diameters b.) Non-contact AFM image showing the height profile of a suspended membrane, c.)Schematic image of the AFM experiment, d.) AFM image of the fractured membrane, e.) Force vs deflection curve of the model and the experiment[2]

They also proposed a mathematical model to understand this nonlinear elastic behaviour and obtain the Young's modulus of the graphene membrane. The nonlinear elastic response was approximated as:

$$F = {\sigma_0}^{2D}(\pi a)(\frac{\delta}{a}) + {E}^{2D}(q^3 a)(\frac{\delta}{a})^3 \tag{2.1}$$

where F is the force applied, a is the membrane diameter, δ is the deflection at the assumed centre point, q is a dimensionless constant which depends on the Poisson's ratio (ν) $q = 1/(1.05 - 0.15\nu - 0.16\nu^2)$ and ${\sigma_0}^{2D}$ is the pretension in the membrane. The AFM nanoindentation of the drums was

performed on multiple samples and with different indenters to obtain a substantial result regarding the model. The load-deflection behaviour of the repeated loading and unloading cycle showed that there exists no slippage in the membrane. Apart from this, a mean value of 342 N/m was obtained for the 2D Young's modulus of the graphene, which approximates to a 3D Young's modulus of 1TPa when assuming a thickness of 0.355nm. The same nanoindentation procedure was done to obtain the fracture strength of graphene, where the force was applied until failure. But, they use a linear model to obtain the breaking strength, which overestimates the value to be 55 N/m.

Lopez-Polin et al.[23] also used the model mentioned above to understand the relationship between the Young's modulus and the defect density present in the graphene membrane. They found an increase in the in-plane stiffness up to 550 N/m for a defect density of ~ 0.2%, after which the in-plane stiffness decreased linearly. They reasoned out this increase to the suppression of the long-wavelength fluctuations due to the presence of defects. On the other hand, the failure strength of the graphene membrane was examined by Huang et al.[61] using the same AFM nanoindentation experiment. They were able to study the effect of grain boundaries on the failure strength of the membrane. The membrane fractured and the crack propagated along the grain boundaries present in the membrane as shown in figure 2.26. The fracture occurred at a load of ~100 nN, which is lower than the typical fracture loads by an order of magnitude, and this indicates that the grain boundaries severely soften the graphene sheets.

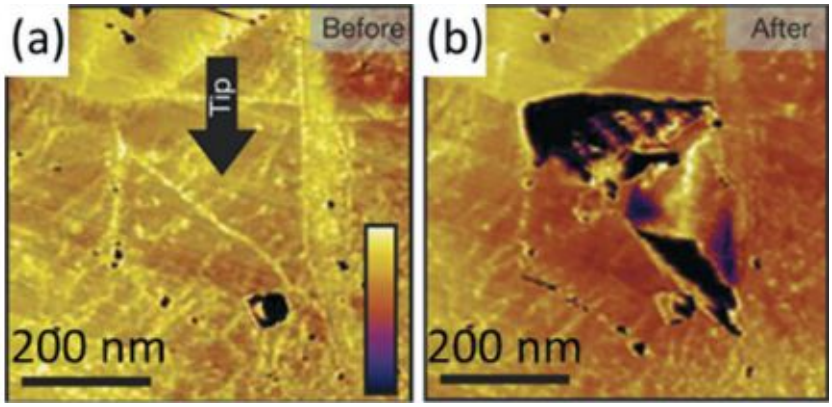

Figure 2.26: AFM images of the graphene grain before (a.) and after (b.) the failure, a.) also shows the point of indentation at the center of the grain boundary[61].

2.4.2. *In situ* measurements using SEM

In situ measurements are a testing method in which the measuring device is placed within a microscope (SEM or TEM). The advantage of in situ measurements is that the deformation and the crack propagation of the graphene membrane can be observed under the microscope. Suk et al.[62] performed an in situ indentation experiment in SEM to study the failure of polycrystalline graphene membranes. The AFM cantilever was used as a force sensor and a nano manipulator that loads the membrane. They were able to obtain precise control over the tip position and also observe the fracture during the indentation because of the in situ setup. The authors observed results similar to Huang et al.[61], where the presence of grain boundaries led to the softening of the graphene membranes.

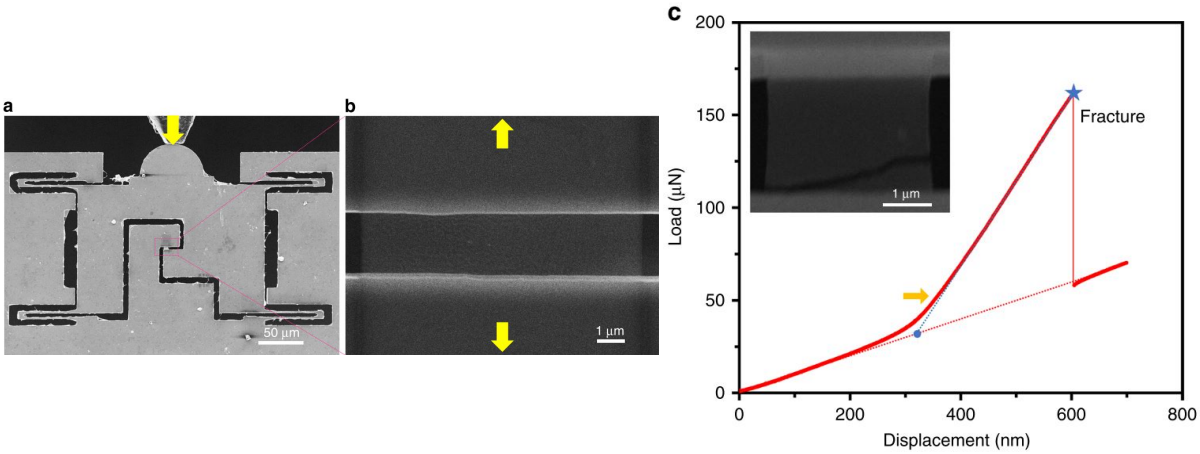

Figure 2.27: a.) SEM image of the micromechanical device with the direction of applied force, b.) Magnified SEM image of the free standing graphene, c.) Load-displacement curve until fracture (blue dotted line indicates the linear fit of the graphene membrane after the reaching the fully stretched configuration)[63].

Cao et al.[63] used a micromechanical device (fig:2.27a) to perform the in situ tensile test of free-standing CVD grown graphene in a SEM. The graphene membrane was cut using the Fusion ion beam cutting process and then transferred onto the trench in the micromechanical device. Force was applied on the micromechanical device with a pico-indenter as shown in figure 2.27(a.). The indenter transducer was used to measure the load and displacement, and the video feed or image sequences from the SEM was used to calculate the tensile strain. The authors obtained a value of ~1 TPa for the Young's modulus, which agrees with the earlier theoretical and experimental predictions[2], and the maximum strain was ~ 6%. However, the fracture strength obtained was ~60 GPa, which is much lesser than the ideal strength of monolayer graphene. This reduction was attributed to the formation of edge defects during the FIB cutting process.

2.4.3. Micro/Nano Electro-Mechanical Systems

Micro/Nano Electro-Mechanical Systems (MEMS/NEMS) are micro/nano-sized systems fabricated for various requirements. These systems function based on some of the fundamental principles like electrostatic force, thermal expansion coefficient, Joule's thermal law or other basic principles. Chemical deposition, electron beam lithography and ion beam lithography are some of the high-end fabrication processes of these MEMS/NEMS devices.

H.Garza et al.[64] used a MEMS tensile testing device to obtain the maximum strain that can be induced into the graphene membranes. The MEMS device works on the principle of Joule's law of heating, where the device possesses contact pads to which the structure of the device is connected, and when electric current flows through the structure, the structure starts to expand. The structure can be arranged suitably to obtain a uniaxial motion of the structure as seen in figure 2.28(b.).

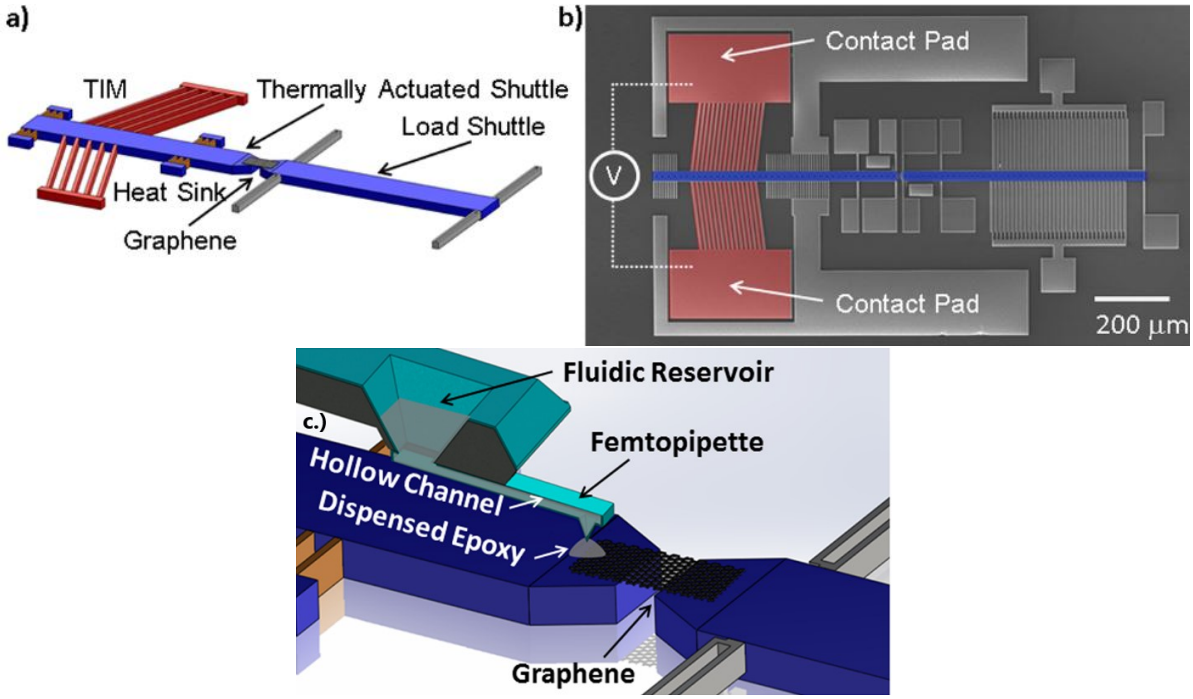

Figure 2.28: a.) Schematic illustration of the MEMS device, indicating the main components b.) SEM image of the entire device, c.) Controlled dispensing of epoxy on the edges of the membrane to obtain better clamping[64]

The clamping of the graphene layer to the shuttle was done in a controlled manner, where fresh epoxy was dispensed using a femtopipette on the overlapping part of the graphene and the shuttles. The epoxy gets chemically bonded to the graphene layer via the amine linkers, which bond with the -COOH or -OH groups. When placed in ambient conditions, these groups are present on the periphery as they replace the dangling bond in the lattice. Multiple cycles of tensile and compressive strains were applied, and no hysteresis was obtained, attributing to no slippage. The authors were able to obtain a maximum strain of ~12.5%, which was mainly attributed to the clamping of the membrane. They also studied the effects of strain on the membrane with Raman Spectroscopy.

2.4.4. Bulge Test by Pressure Difference

Bulge test is a form of mechanical testing in which the suspended membrane is forced to deflect out-of-plane to form profiles similar to blisters. A pressure difference or electrostatic gating can impose these deflections. Generally, these deflections are measured using a calibrated optical microscope, laser interferometry or even AFM[65].

The mechanics of a graphene membrane that was subjected to strain was studied by Lopez-Polin et al.[66] by straining the membrane by providing a pressure difference as shown in figure 2.29(I,II). The advantage of the pressure difference induced strain is that the strain is uniformly distributed in the membrane. An AFM nanoindentation setup was used to study the Young's modulus of the strained membrane. The total strain induced in the membrane has contributions from the bulging of the membrane, residual strain from the growth or transfer of the membrane and the local stress induced by the indentation tip. The load-deflection curve obtained experimentally (fig:2.29(III.)) did not agree with the model proposed by Lee et al.[2](eq:2.1), so simulations were performed to understand the mechanics. The authors suggest that the complete third-order polynomial model given by Lin et al.[67] deals with the problems associated with the model in equation 2.1. The results obtained showed an increase in the in-plane stiffness of the membrane subjected to strains greater

than 0.25%, and they attributed this to the suppression of the thermal fluctuation.

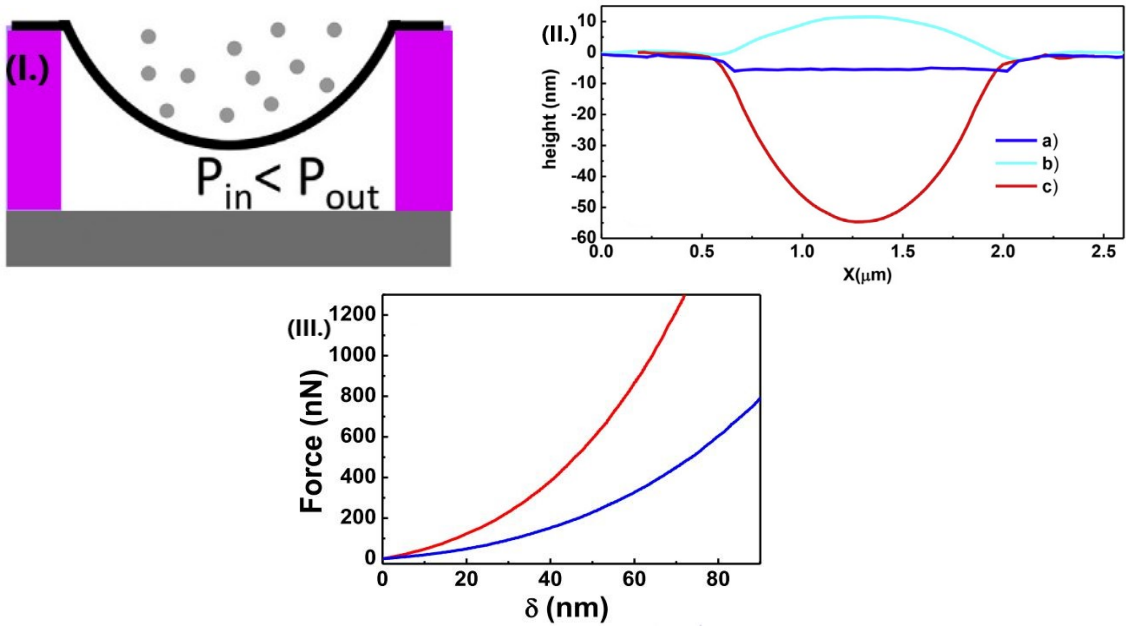

Figure 2.29: I.) Schematic illustration of bulge created by pressure difference, II.) AFM profiles of (a.) P_{in} =P_{out} (b.) P_{in} >P_{out} (c.) P_{in} <P_{out}, III.) Load-displacement experimental curves of membrane at 0 atm (blue) and 4 atm (red).[66]

Hwangbo et al.[68] studied the fracture characteristics of a CVD grown graphene membrane by using the same setup as mentioned above (fig:2.30). They used O-rings to avoid the leakage of pressure, which might lead to errors in the results. A high-speed camera was used to visualise the failure of the membrane that took place in less than 2 ms. The failure appeared to be due to the subcritical crack growth in ambient conditions.

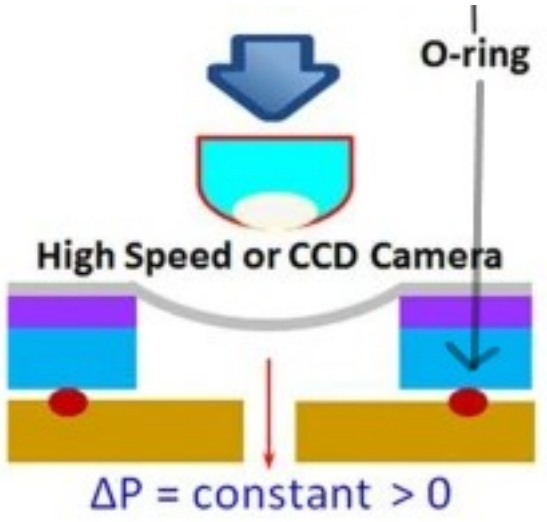

Figure 2.30: Schematic illustration of the experimental setup with the high speed camera[68].

2.4.5. Electrostatic Gating

Electrostatic gating is an actuation method where the graphene drums are electrostatically deflected by applying a voltage across the graphene membrane and a gating chip present below the

membrane. Compared to the bulge test by pressure difference, no issue exists related to the weak clamping or leakage. The voltage can be applied to the back gate by using contact pads fabricated on the substrate.
Wong et al.[69] used the principle of electrostatic gating to deflect the suspended graphene drums (fig:2.31). The deflection produced by the gating voltage was measured using an AFM, where the initial profile was scanned before applying the voltage. After which, the voltage was applied, and the corresponding deflection was scanned. The authors considered the effective deflection due to the applied voltage to be obtained by subtracting the profile of the membranes before and after applying the voltage. These results were fit to the plate theory in order to obtain the elastic modulus. The force applied by the electrostatic gate was calculated using the parallel plate equation for a uniformly distributed load, which is as follows:

$$F = \frac{\epsilon_0 \epsilon_r A V_s^2}{2(g - d_0)^2} \tag{2.2}$$

where ϵ_0 = 8.854 x $10^{-12} F/m$ is the permittivity of free space, ϵ_r is the relative permittivity of the membrane, A is the area of the suspended graphene drum, V_s is the voltage applied to the back gate, g is the gap between the graphene drum and the back gate after subtracting the initial sag and d_0 is the peak deflection of the graphene drum. In order to understand and compare the force-displacement behaviour, an analytical model based on the deflection of circular plates and a finite element simulation were carried out. Interestingly, the three results were in total agreement with each other only when the deflection mode was purely parabolic. This variation was attributed to the assumptions present in the circular plate model.

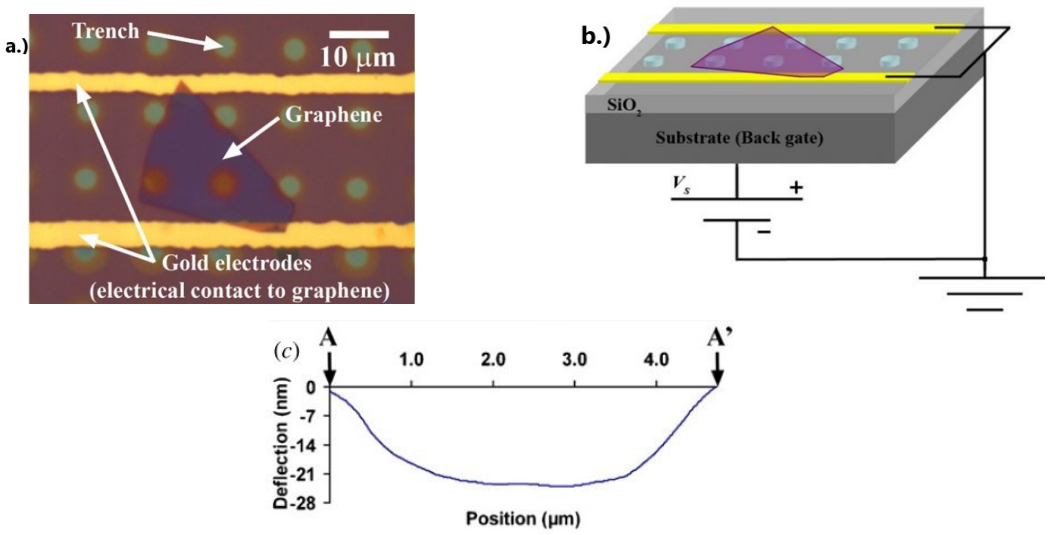

Figure 2.31: a.) Optical image of the substrate with indication of the important components, b.) Schematic illustration of applying gate voltage, c.) Graph of height variation of the entire drum (deflection mode shape).[69]

A similar experimental setup was used by Nicholl et al.[32], where the electrostatic gate was used to deflect the graphene membrane. An interferometric profilometry method was used together with the electrostatic gate to measure the maximum out-of-plane deflection experienced by the membrane (Fig:2.32(a.)). Multiple samples were used to get a statistical understanding of the obtained results. The experimental work was done to understand the effect of crumpling on the mechanics of the suspended graphene membrane. The results obtained showed a drastic reduction in the in-plane stiffness ranging from 20 N/m to 100 N/m, far less than the expected value of 340 N/m (pristine graphene).

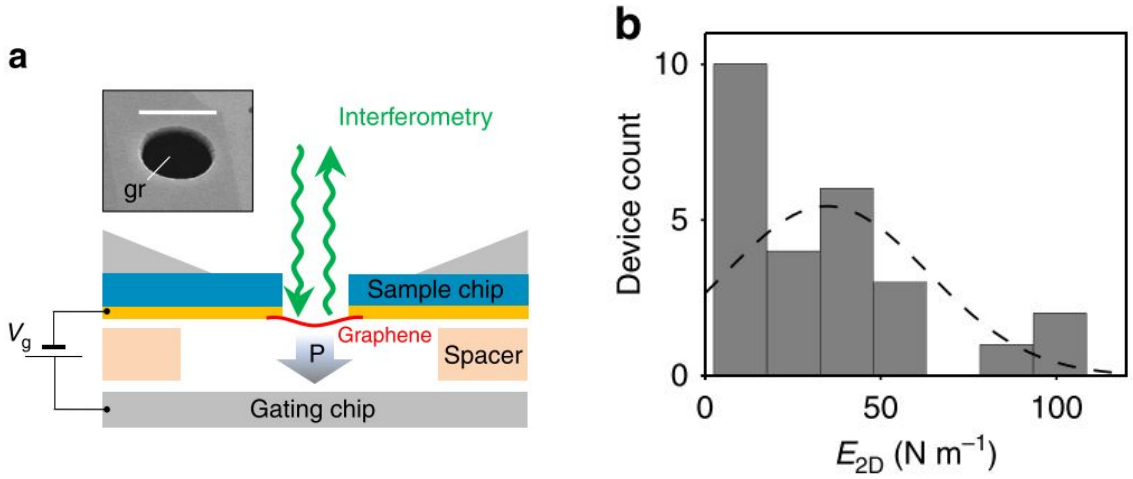

Figure 2.32: a.) Schematic illustration of the experimental setup, inset: SEM image of the graphene drum , b.) Statistical histogram of the obtained in-plane stiffness of the multiple drums measured.[32]

3

Research Question and Objective

The previous chapter deals with a detailed literature study on the properties of graphene, the imperfections present in the membranes and the different fabrication, transfer and measurement techniques used to study the mechanics of graphene. Based on this study, we can say that graphene possesses exceptional properties and have a large field of applications possible. However, a need for experimental validation of some of the theoretically obtained properties still exists. This is because the experimental validations are hindered by the presence of structural and surface imperfections. Some experimental works have been done to understand the effects of some of the imperfections. Experimental results have been obtained to show the effect of point defects[23] and line defects[61]. However, experimental results based on static wrinkles or crumples are yet to be obtained entirely. Apart from the need for experimental results, crumpled graphene is said to have some applications of its own like strain sensing, electrodes for supercapacitors and energy storage [3]. These observations make crumpled graphene an exciting aspect of graphene to study about.

The different methods of probing the mechanics of the graphene membrane were also discussed in the previous chapter. It is evident that all the discussed methods have advantages of their own. It is recommended to select the testing method based on the requirement and availability of the setup. Atomic force microscope (AFM) nanoindentation is regarded as one of the pioneer methods to obtain properties like Young's modulus and breaking strength. Moreover, analytical models and simulations based on the AFM nanoindentation method are accepted by most. These advantages make AFM nanoindentation a preferred choice.

Based on these findings, the main objective of this research is to experimentally understand the effects of crumpling on the mechanics of a monolayer graphene membrane by probing the membrane at the centre using the cantilever tip of the AFM.

In order to achieve the set objective of this research, the main research question needs to be answered. The main research question is as follows:

How does the presence of crumples affect the pretension and 2D Young's modulus of the graphene membrane ?

An additional sub-question could also be looked into: What happens to the crumples present in the membrane when the cantilever tip indents the membranes?

4

Research Methodology

The motivation behind this chapter is to put forth the methodology behind the entire thesis one after the other. The chapter deals with the fabrication of the flat and wrinkled graphene samples and also the probing technique used to extract the mechanical properties of the the samples.

4.1. Fabrication of Samples

The different types of fabrication methods generally used to obtain graphene films were discussed in the previous section. The literature clearly shows that for laboratory/research purposes, CVD graphene is the most preferred due to the quality of the graphene film obtained. However, the transfer of the CVD graphene is also essential as the quality can easily be affected by the parameters or steps during transfer. The previous section also deals with the different transfer methods used to transfer CVD graphene onto target substrates. The two categories, etching and etching-free transfer of graphene, were discussed, and from that, we can say that the use of the etching transfer is less complex compared to the etching-free transfer, but etching transfer requires more care and skill to make sure that the transfer is both intact and clean. The suspended graphene samples used in this article have been fabricated based on the idea of etching transfer, and the procedure has been discussed below.

Graphene Transfer

Initially, five petri dishes filled with 0.5 Molar (M) ammonium persulphate solution (APS) were prepared. To four of the petri dishes containing 0.5M APS, 0.1% liquinox of different quantities (5, 10, 20, 30 μl) are added while the fifth petri dish is left undisturbed. Simultaneously, two separate petri dishes are taken, one filled with 2 M APS and the other filled with ultra-pure distilled water. Graphene films with the copper foil on which they were chemically grown (approximate size of 1 x 1 cm^2) are prepared and first placed on the surface of the 2 M APS etchant. The film is then transferred onto the petri dish containing distilled water for cleansing. Placing the samples in 2 M APS followed by distilled water is repeated a few times to ensure that the copper foil on the backside is effectively etched away. Once the solution starts to turn blue, indicating the copper foil's dissolution, the samples are then transferred onto the five petri dishes containing 0.5 M APS.

Figure 4.1: Image of two pieces of graphene along with the copper foil floating on the surface of the APS solution in separate petri dishes.

Liquinox is added to the 0.5M APS to increase the surface pressure of the etchant solution. The increase in surface pressure acts as a compressive force from all directions on the graphene film, which causes the film to crumple or form wrinkles. Over some time, the entire copper foil is dissolved in the APS solution, leaving behind only the graphene foil in all the petri dishes. In order to have a clean and intact transfer, it is necessary to clean the film with distilled water. This is done to mitigate the influence of the APS solution or liquinox on the graphene film. Since the procedure does not use any support layer like PMMA, the film cannot be physically removed from the petri dish to rinse it in distilled water. In order to deal with this, the APS solution and the liquinox were slowly removed from the petri dish using a microliter syringe, and the solution was replaced with distilled water. The switching of liquids was done several times to ensure that only a bare minimum of the APS solution remains. The entire switching procedure was done carefully and away from the film to ensure that the film was not affected by this. The films are then let to rest in distilled water for some time before transferring onto the target substrate. The films are transferred to different Si/SiO_2 substrates by gently placing the substrate in contact with the graphene film. The entire workflow of the transfer method is illustrated in fig 4.2.

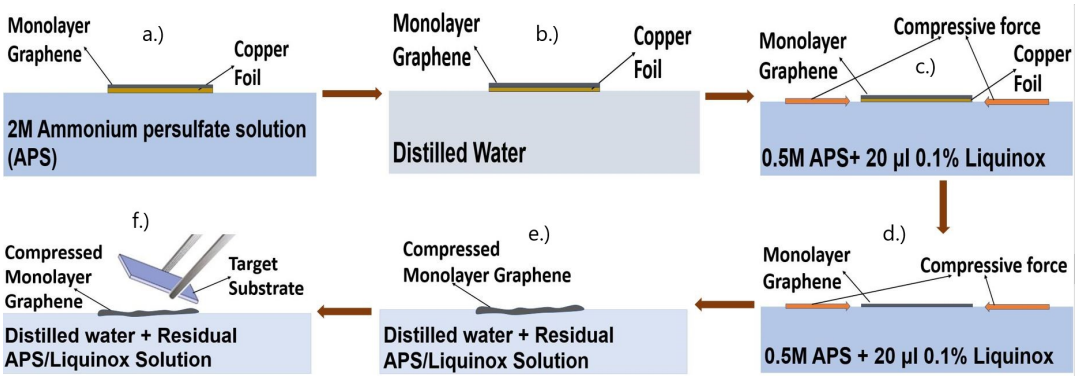

Figure 4.2: An illustration of the complete procedure involved in the transfer process. a.) Film placed in 2M APS, b.) Film rinsed in distilled water, c.) Film transferred to the 0.5M APS solution containing 0.1% liquinox, d.) Removal of copper foil by etching, d.) Replacing APS solution and liquinox with distilled water, e.) Transferring film to the target substrate.

The substrates are then let to dry at atmospheric conditions naturally. The substrates used have through holes and not cavities. During the transfer, there is a high probability of distilled water being trapped between the graphene film and the substrate, and by using substrates with through holes, the aqueous medium can be removed by natural drying or by heating the substrate using a

hot plate. Whereas, in the case of cavities, the aqueous medium stay trapped inside them and is likely to affect the film during measurements.

4.2. Imaging of Samples

Optical images of the graphene films suspended on the Si/SiO_2 substrates were obtained using the Keyence Digital Microscope VHX-6000 with a 2000x magnification. The optical images were taken to check for the existence of graphene membranes. The optical images revealed that in the case of 5 and 10 μl of 0.1% liquinox added, the wrinkling of the graphene membranes was not very clear compared to the case of 20 μl 0.1% liquinox. Whereas, in the case of 30 μl 0.1% liquinox, the film was not transferred, which could be due to the film's breakage into fragments that could not be transferred. The fragmentation of film is even visible in the case of the sample with 20 μl 0.1% liquinox as seen in fig 4.3 (left). The optical images show the clear difference between the two sets of samples, one without the addition of liquinox (fig 4.3 centre) and the other with the addition of 20 μl 0.1% liquinox (fig 4.3 right).

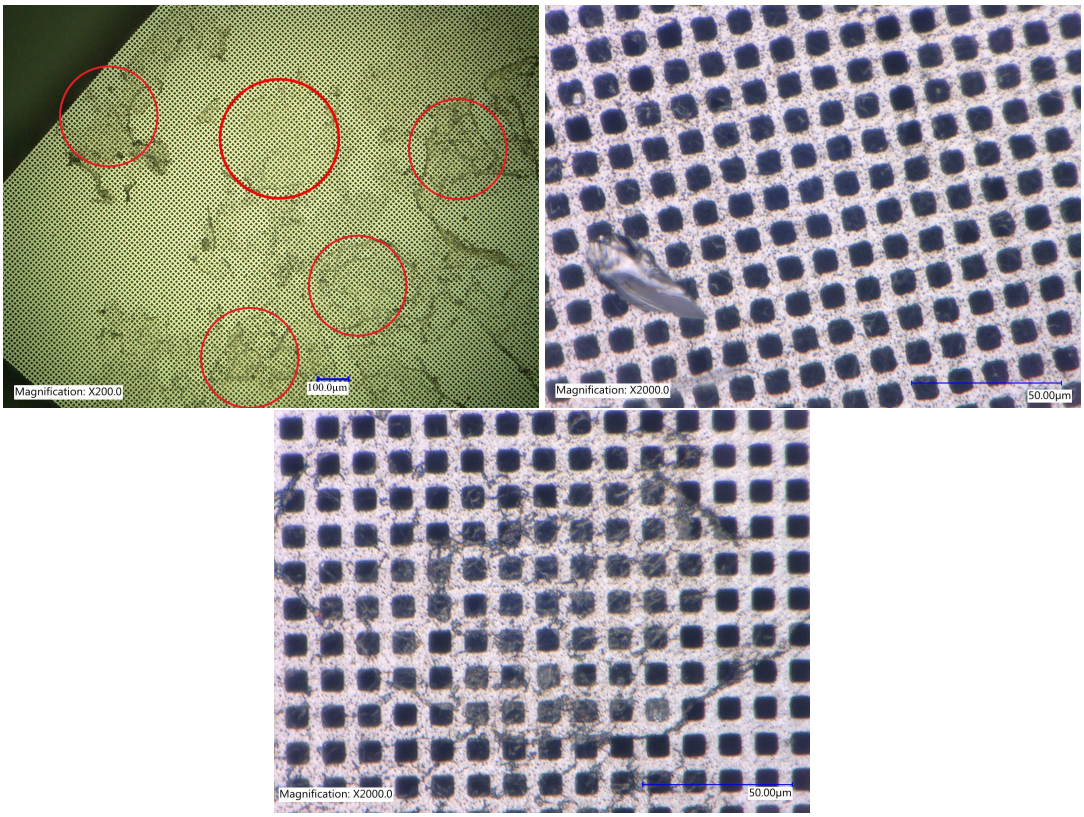

Figure 4.3: Optical Images of (Top-Left.) Substrate showing the fragmentation of the graphene film during the transfer, (Top-Right.) Suspended graphene membranes without the influence of liquinox , (Bottom.) Suspended graphene membranes with the influence of liquinox.

The membranes are then placed under a scanning electron microscope (SEM) to obtain the images of the membranes at higher resolutions. The SEM is also used to distinguish the features present in each membrane. The SEM images of a flat graphene membrane and a heavily crumpled membrane are shown in fig 4.4. The features present in both membranes can be seen distinguishably. The SEM image (fig 4.4 (right)) clearly show that by the addition of liquinox, the membrane gets heavily crumpled in the out-of-plane direction. However, one shall expect the membrane with-

out the influence of liquinox to be perfectly flat and have no structural irregularities. However, fig 4.4 (left) shows that the membrane is not perfectly flat, and this may be because no supporting layer was used during the transfer. Lack of supporting layer can cause the APS solution to affect the film structurally and form static wrinkles or crumples. Although, a clear difference between the amount of crumpling in both the samples can be seen in the SEM images.

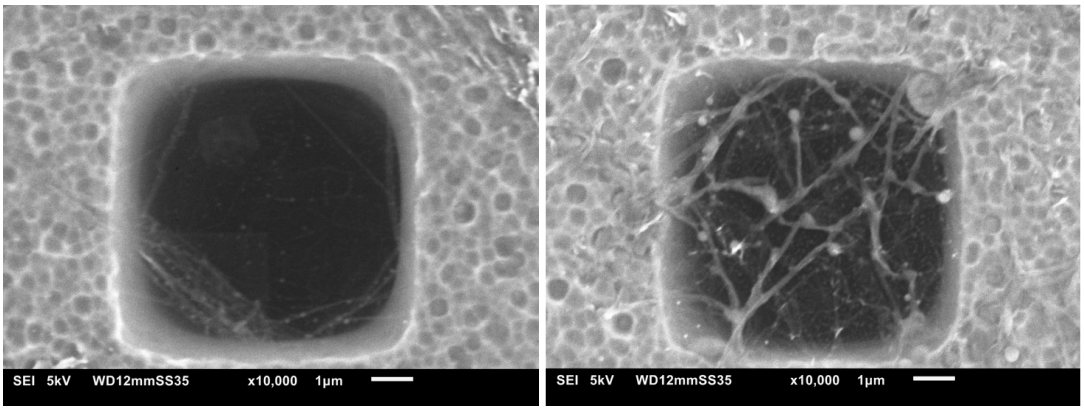

Figure 4.4: SEM images of (Left.) a flat graphene membrane, (right.) a heavily crumpled graphene membranes.

However, the optical or the SEM images cannot be used to check if the membranes are actually suspended. In order to counter this, the membranes are then imaged using an atomic force microscope (AFM).

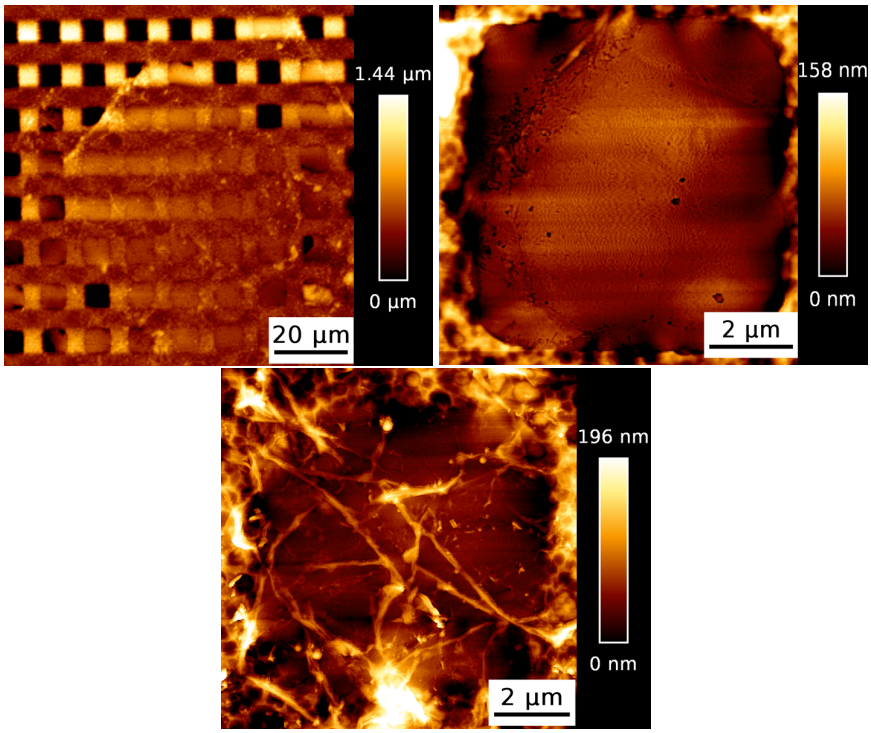

Figure 4.5: AFM AC mode images of (Top-Left.) A region of graphene membranes to show that the membranes are suspended, (Top-Right.) suspended flat graphene membrane, (Bottom.) suspended heavily crumpled graphene membrane.

The AFM imaging is done using a JPK NanoWizard 4 NanoScience AFM, and the images are processed using the JPK SPM Data Processing Software. The imaging was performed using a silicon

cantilever (NCLR, Nanoworld) coated with aluminium (detector side). The nominal resonance frequency of the cantilever is around 170 kHz, and the spring constant is around 30 N/m. The AFM was operated in the AC/tapping mode at room temperature to obtain the images. The resolution of the images obtained was 512 x 512 pixels. The topology obtained from the scanning of the AFM cantilever shows that the membranes are suspended, and in addition, the features of each membrane can be seen clearly. The AFM images of the same two membranes as in SEM are shown in fig 4.5 (the orientation of the images could be misleading). The comparison between the SEM and AFM images of a membrane helps better understand the membrane's features. The fact that the features present in the membranes are seen clearly in both SEM and AFM suggests that the depiction obtained from the AFM is reliable, and observations based on the topography of the AFM images can be made. Alternatively, AFM imaging is also used to obtain the location of the centre point of the membranes. At this point, the set value of force is applied to extract the mechanical properties.

4.3. Probing the Mechanical Properties of the Sample

The nanoindentation of the membranes is done in contact mode using the JPK NanoWizard AFM. The point at which a membrane is indented is based on the centre located using the AFM image of the membrane. The z-length/approach distance, the speed at which the indentation is done and the maximum force applied on the membrane are preset before the indentation. With these preset parameters, the membrane is indented three times, which means three complete cycles of approach and retract. The three sets of data points collected from the indentation are processed to obtain the pretension (linear stiffness) and the 2D young's modulus (second-order elastic stiffness) of the membrane.

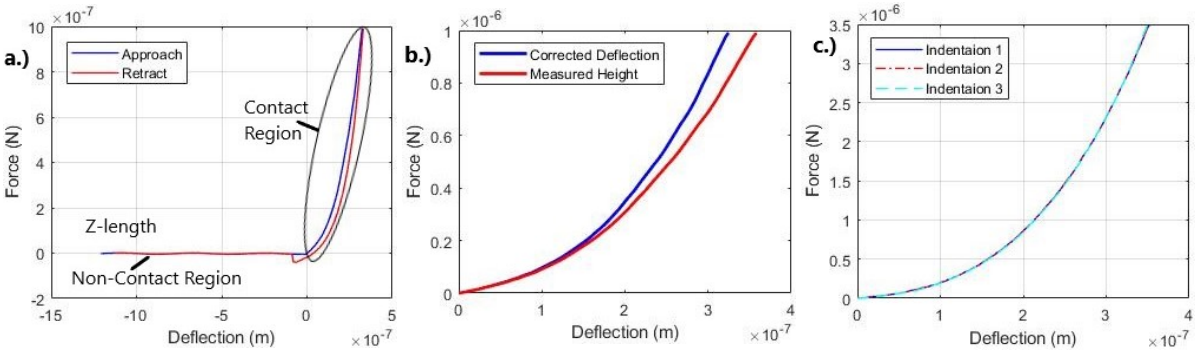

Figure 4.6: a.) Typical Force-Deflection plot obtained for one of the membranes. The plot shows the z-length, contact and non-contact regions and the approach and retract curves of a single indentation, b.) Comparison plot showing how the Force-Deflection plot changes by correcting the deflection of the cantilever by accounting for the bending of the cantilever, c.) Comparison plot between the 3 indentations on the sample membrane.

A typical force-deflection plot containing both approach and retract curves obtained from one of the membranes is shown in fig 4.6a. Two distinct regions can be seen in the plot, and they are the non-contact region and the contact region. The contact region is the region of interest used to extract the mechanical properties. It is important to note that the deflection obtained from the AFM is the z-scanner(piezo) readout and not the actual deflection of the membrane. In order to obtain the actual deflection (δ) of the membrane, it is essential to account for the cantilever bending. The bending of the cantilever is accounted for by subtracting the cantilever deflection (d) from the Z-scanner(piezo) readout (D) as in eq4.1.

$$\delta[nm] = D[nm] - d[nm] \tag{4.1}$$

The cantilever deflection (d) can be obtained by taking the ratio of the voltage readout from the

photosensitive diode (PSD) to the sensitivity of the cantilever (S).

$$d[nm] = \frac{PSD[V]}{S[\frac{V}{nm}]} \tag{4.2}$$

A clear difference can be seen (fig 4.6b) between the force-deflection curves before and after the correction to account for cantilever bending. On the other hand, the force-deflection curve of the three sets of indentation is compared as shown in fig 4.6c. The comparison shows that the nanoindentation experiment is repeatable, which implies no slippage exists between the membrane and the substrate.

In order to extract the values of pretension and 2D Young's modulus from the force-deflection curves, the AFM indentation experiment is generally modelled as a circular clamped membrane with a point load at the centre [2]. However, since the membranes in hand are square, the obtained model has to be altered to account for the shape of the membrane. Wang et al.[70] developed a force-displacement relation for rectangular membranes. The relation can be considered as a sum of two parts as in eq 4.3.

$$F = F_{\sigma}(\delta) + F_{E_{2D}}(\delta) \tag{4.3}$$

where F is the effective force experienced by the membrane, F_{σ_0} is the force due to the axial tension in the membrane, $F_{E_{2D}}$ is the force due to the large deformation and δ is the deflection in the membrane. The first term, F_{σ_0}, is linearly dependent on the deflection of the membrane and this relation is expressed in eq 4.4.

$$F_{\sigma}(\delta) = \sigma_0(\pi R_{equ})\beta^{1/2}(\frac{\delta}{R_{equ}}) \tag{4.4}$$

where σ_0 is the pretension or linear stiffness of the graphene membrane, r is the radius of the indenter, R_{equ} is the equivalent radius of the rectangular membrane ($R_{equ} = (l * b/\pi)^{1/2}$), l and b are the length and breadth of the membranes, and β is the aspect ratio. The second term, $F_{E_{2D}}$, is dependent on the deflection in a nonlinear manner, and the relation is expressed in eq 4.5.

$$F_{E_{2D}}(\delta) = E_{2D}(q^3 R_{equ})\beta^{1/2}(\frac{\delta}{R_{equ}})^3 \tag{4.5}$$

where E_{2D} is the 2D Young's modulus or the second-order elastic stiffness of the graphene membrane and q is a non-dimensional quantity related to the Poisson's ratio (γ), q = $1/(1.05\text{-}0.15\gamma\text{-}0.16\gamma^2)$. Simulations were performed by Lee et al.[2] to study the influence of the indenter radius on the force-deflection behaviour of the membrane. It was noted that for $r << R_{equ}$, the force-deflection behaviour is not affected by the indenter radius. In the case of our research, square membranes are used, so the aspect ratio becomes β= 1, and the equivalent radius becomes $R_{equ} = (l/(\pi)^{1/2})$, where l is the length of the square membrane. The entire force-deflection relation can now be rewritten as,

$$F = \pi\sigma_0(\delta) + \frac{q^3 E_{2D}}{(R_{equ})^2}(\delta)^3 \tag{4.6}$$

5

Paper: The effect of crumpling on the mechanics of monolayer graphene

The Effect of Crumpling on the Mechanics of Monolayer Graphene

R.Prasad , F.Alijani , G.J.Verbiest , H.Arjmandi-Tash , H.Liu

***Abstract*—Graphene is considered the strongest material measured, but it is crumpled in the out-of-plane direction in most practical situations due to its low bending rigidity. We investigate the consequences of this crumpling on the effective mechanical constants of graphene. In this study, two types of graphene membranes are considered, one is a flat membrane, and the other is a heavily crumpled membrane. The atomic force microscope nanoindentation experiment is performed to determine the mechanical response of the membranes. We find the 2D Young's modulus (E_{2D}) of flat graphene to be 140 $\pm$ 44 N/m at room temperature, which is much lesser than the expected 340 N/m (from previous studies). Meanwhile, the E_{2D} of heavily crumpled graphene is found to be 393 $\pm$ 145 N/m, which indicates a slight hardening of the sample. However, the results obtained are contrary to the previous works, which points towards the decrease of in-plane stiffness when the crumpling is increased. In this work, the transformation of the crumples when subjected to tensile loading is also observed. The variation in the results could provide a different dimension in pristine or crumpled graphene applications. However, further research into the intrinsic strength and Young's modulus of these crumpled membranes is required to validate the possible applications.**

KEYWORDS: Graphene, Atomic Force Microscope, Crumples, Pretension, 2D Young's modulus

I. Introduction

Over the years, graphene has been considered a prominent two-dimensional (2D) material as it possesses excellent properties and has a vast area of applications. Graphene exhibits high intrinsic strength, thermal and electrical conductivity and high transmittance [1], [2], [3], [4], which makes the material ideal for applications like mechanical reinforcements in nanocomposites, protective coating, mechanical transduction, electronic transistors, flexible displays, energy storage systems, etc[5], [6], [7], [8], [9]. Theoretical and experimental studies show that the 2D Young's modulus and tensile strength of graphene are about 340 N/m and 130 GPa, respectively, which makes graphene the strongest material measured[2]. The perfect 2D (sp^2 hybridized) lattice structure of graphene is the primary reason for these exceptional properties and applications. However, obtaining graphene films with this perfect lattice structure has been a monumental task on its own. Studies have shown that, in realistic scenarios, graphene possess defects in the lattice structure or have surface corrugations in the out-of-plane direction[10], [11], [12].

When considering the irregularities as mentioned above, the effects of the structural defects (point defects, edge defects, grain boundaries) on the in-plane stiffness and strength of the graphene film have been primarily studied theoretically, and the studies point towards the degradation of the film[11]. Similarly, the effects of the surface corrugations (ripples, wrinkles, crumples) on the mechanical properties of graphene are only studied theoretically, and these theoretical studies show that the in-plane stiffness and tensile strength of graphene films decrease in the presence of the surface corrugations [10], [13], [14]. However, the lack of experimental validation of these theoretical results urges the need for experimental studies on the effects of these surface corrugations.

Since, in most cases, graphene is crumpled in the out-of-plane direction due to its low bending rigidity, Nicholl et al.[14] experimentally studied the effects of these crumples on the mechanical properties of graphene. The crumpling of graphene is primarily due to static wrinkling and dynamic crumpling. The effects of the two mechanisms were studied, and the results showed that the effect of the out-of-plane flexural phonons on the in-plane stiffness of graphene is negligible and that the effect of the static wrinkles is dominant[14]. The formation of these static wrinkles has been thoroughly studied over the years. According to research, the static wrinkles are generally formed due to the uneven stress distribution during the transfer of graphene films, polarity difference in the thermal expansion coefficient (TEC) between the growth substrate and the graphene film during chemical vapour deposition (CVD) or the additional stresses induced due to the morphology of the growth or target substrate[15], [16], [17]. In addition, Bao et al.[18] have managed to induce controlled and oriented wrinkles on the graphene film by making use of the polarity difference in the TEC between the film and the substrate. These studies make the experimental study of the effects of static wrinkles or crumples more intriguing and looked into.

In this article, we perform a quantitative study to understand the effect of crumples on the in-plane stiffness of the graphene membrane. Two sets of films are transferred onto separate target substrates for this purpose, Sample (A) - CVD graphene, Sample (B) - CVD graphene subjected extensive crumpling with the addition of liquinox. In order to extract the mechanical response of the samples fabricated, the membranes are probed using the atomic force microscope (AFM). The tip of the AFM cantilever is used to image as well as perform nanoindentation at the centre of the graphene membranes. Based on the force-deflection behaviours obtained from the nanoindentation measurements, the mechanical constants, pretension (σ_0) and 2D Young's modulus (E_{2D}) were obtained and discussed. The AFM images show that the graphene membrane is not completely flat in the case of CVD graphene (sample A). The mechanical constant obtained for the CVD graphene shows a softening behaviour (E_{2D} = 140$\pm$44N/m) and are in agreement with the results obtained by Nicholl et al.[14].

Meanwhile, in the case of the heavily crumpled graphene (sample B), the AFM images depict the membranes to be far more crumpled. However, the mechanical constants obtained do not show any softening behaviour and, on the contrary, shows a marginal hardening behaviour (E_{2D} = 393±145 N/m). The following sections provide an understanding of the observed results and also the possible explanations for these contradictory results. After the nanoindentation, the membranes are imaged again to understand how the membrane deforms after the indentation.

II. Methodology

A. Fabrication of Samples

Initially, two petri dishes filled with 0.5 Molar (M) ammonium persulphate solution (APS) were prepared. To one of the petri dishes containing 0.5M APS, 20 μl of 0.1% liquinox (Sample B) is added while the other petri dish (Sample A) is left undisturbed. Simultaneously, two separate petri dishes are taken, one filled with 2 M APS and the other filled with ultra-pure distilled water. Graphene films with the copper foil on which they were chemically grown (approximate size of 1 x 1 cm^2) are prepared and first placed on the surface of the 2 M APS etchant. The film is then transferred onto the petri dish containing distilled water for cleansing. Placing the samples in 2 M APS followed by distilled water is repeated a few times to ensure that the copper foil on the backside is effectively etched away. Once the solution starts to turn blue, indicating the copper foil's dissolution, the samples are then transferred onto the two petri dishes containing 0.5 M APS.

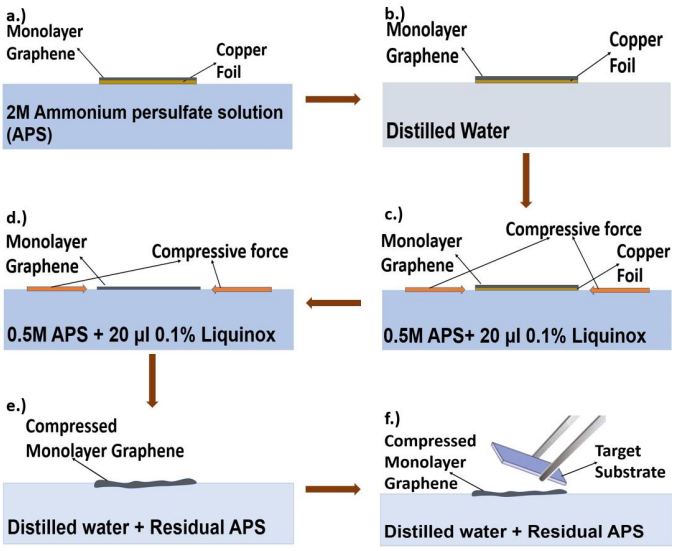

Fig. 1. An illustration of the complete procedure involved in the transfer process. a.) Film placed in 2M APS, b.) Film rinsed in distilled water, c.) Film transferred to the 0.5M APS solution containing 0.1% liquinox, d.) Removal of copper foil by etching, e.) Replacing APS solution and the liquinox with distilled water, f.) Transferring film to the target substrate.

Liquinox, a detergent, is added to one of the petri dishes containing 0.5M APS to increase the surface pressure of the etchant solution. This increase in surface pressure, which is basically the reduction of surface tension, acts as a compressive force from all directions on the graphene film, which causes the film to crumple. Over time, the entire copper foil is dissolved in the APS, leaving behind only the graphene foil in both the petri dishes. The APS and the added Liquinox are then slowly removed from the petri dish using a microliter syringe, and the solution is replaced with ultra-pure distilled water. The switching of liquids was done several times to ensure that only a bare minimum of the APS solution remains. The films are then let to rest in distilled water before transferring onto the target substrate.

The films are transferred to different Si/SiO_2 substrates by gently placing the substrate in contact with the graphene film. The graphene film is suspended over square through holes (8 x 8 μm^2) present in the substrate. Substrates with through holes are used as they can easily leach distilled water from the substrate to eliminate its influence on the membranes. The substrates are then let to dry at atmospheric conditions naturally. The entire workflow of the transfer method is illustrated in fig 1.

B. Experimental Setup

In a broad sense, Atomic Force Microscope (AFM) works on the principle of surface sensing by using a very sharp tip attached to the silicon cantilever. The tip can be used to image the surface features of a sample with atomic resolution or indent the sample depending on the mode of usage. When the cantilever tip comes in contact with the sample during the measurements, the cantilever bends. This cantilever bending is detected using a laser diode and a photodetector. A schematic illustration of the AFM setup is shown in fig 2.

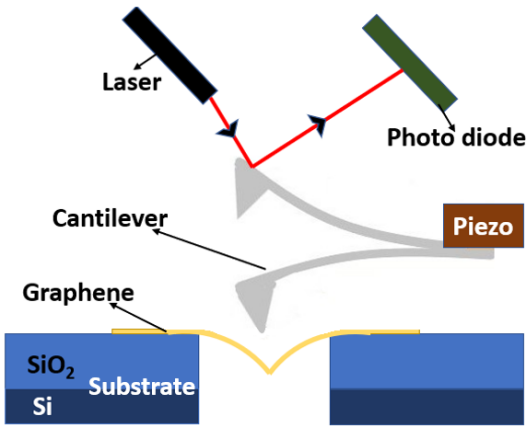

Fig. 2. Schematic image of a nanoindentation setup using an AFM

The membranes fabricated were first imaged using the Tapping/AC mode, wherein a feedback loop has to be set to obtain clear representative images. The topographies of the two sets of samples are traced line by line using the AFM. The initial AFM images of the two samples as shown in fig 3(a-b). The images show a clear difference in the degree of crumpling present in the two samples.

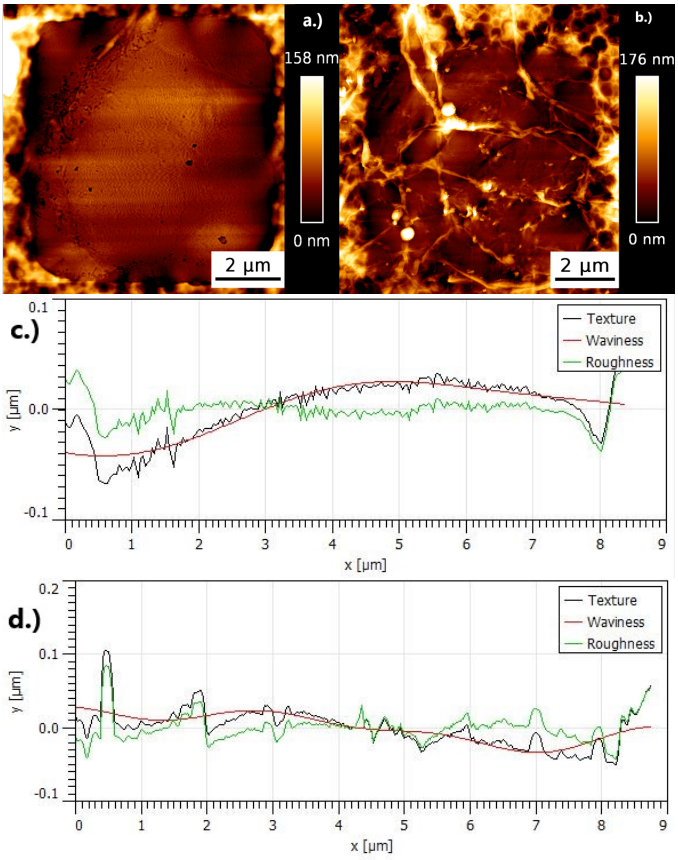

Fig. 3. AFM image of a.) Sample A, b.) Sample B, c,d.) Topology profile of Sample A and B respectively. It also depicts how the waviness of the profile is considered to obtain the roughness of the membranes.

The graphene membranes are then indented at their centre with the AFM cantilever tip. The membranes are indented with a preset value of maximum force, and the corresponding deflection behaviour of the membrane is obtained. In order to obtain the actual deflection (δ) of the membrane, it is essential to account for the cantilever bending [19]. The bending of the cantilever is accounted for by subtracting the cantilever deflection (d) from the Z-scanner(piezo) readout (D) as in eq1.

$$\delta[nm] = D[nm] - d[nm] \tag{1}$$

The cantilever deflection (d) can be obtained by taking the ratio of the voltage readout from the photosensitive diode (PSD [V]) to the sensitivity of the cantilever (S [V/nm]).

C. Extracting the mechanical constants of the membrane

The force-deflection curves obtained from the AFM nanoindentation can be used to extract the pretension (σ_0) and 2D Young's modulus (E_{2D}) of the graphene membrane. In order to extract these values, the AFM nanoindentation experiment is modelled as a rectangular clamped membrane with a point load at the centre. Wang et al.[20] developed a force-deflection relation for rectangular membranes. The nonlinear elastic relation can be considered as a sum of two parts as in eq 2.

$$F = F_{\sigma_0}(\delta) + F_{E_{2D}}(\delta) \tag{2}$$

where F is the effective force experienced by the membrane, F_{σ_0} is the force due to the axial tension in the membrane, $F_{E_{2D}}$ is the force due to the large deformation, and δ is the deflection in the membrane. The first term, F_{σ_0}, is linearly dependent on the deflection of the membrane and this relation is expressed in eq 3.

$$F_{\sigma_0}(\delta) = \sigma_0(\pi R_{equ})\beta^{1/2}(\frac{\delta}{R_{equ}}) \tag{3}$$

where σ_0 is the pretension of the graphene membrane, r is the radius of the indenter, R_{equ} is the equivalent radius of the rectangular membrane ($R_{equ} = (l * b/\pi)^{1/2}$), l is the length of the membrane, b is the breadth of the membrane and β is the aspect ratio. The second term, $F_{E_{2D}}$, is dependent on the deflection in a nonlinear manner and the relation is expressed in eq 4.

$$F_{E_{2D}}(\delta) = E_{2D}(q^3 R_{equ})\beta^{1/2}(\frac{\delta}{R_{equ}})^3 \tag{4}$$

where E_{2D} is the 2D Young's modulus of the graphene membrane and q is a non-dimensional quantity related to the Poisson's ratio (γ), q = 1/(1.05-0.15γ-0.16γ^2). The influence of the tip radius on the force-deflection characteristics was simulated by Lee et al.[2]. They found that when the equivalent radius of the membrane is far greater than the radius of the indenter (R_{equ} >>r), the influence of the indenter on the force-deflection can be neglected and can be considered as a point load. Since the membranes are square in shape, the aspect ratio becomes β = 1 and the equivalent radius becomes $R_{equ} = (l/(\pi)^{1/2})$. The entire nonlinear force-deflection relation can now be rewritten as,

$$F = \pi\sigma_0(\delta) + \frac{q^3 E_{2D}}{(R_{equ})^2}(\delta)^3 \tag{5}$$

III. Results and Discussions

In order to image the membranes, the JPK AFM is used in the AC mode with a feedback loop set to control the amplitude of the tapping motion. The initial AFM topography images of the two types of samples can be seen in fig 3(a-b). A clear difference in the level of crumpling can be seen between the AFM images of the two samples. In the case of sample A, the majority of the membrane area is flat, and this can also be seen in the topology profile of the membrane (fig 3(c)). However, there still exists some out-of-plane deformations. In contrast, the AFM image of sample B is dominated by features in the form of smaller flat areas surrounded by valleys and peaks, which can also be seen in the topology profile (fig 3(d)). These features are the out-of-plane deformations formed due to the compressive force experienced by the membranes by adding liquinox. A closer look at the AFM image of sample B reveals that some of the out-of-plane deformations collapse over each other and

form folds.

The AFM was then used in the contact mode to perform the nanoindentation measurements of the membranes. The force-deflection data points(blue points) of one of the membranes along with its curve fit(red solid line) using equation 5 is shown in fig 4a. E_{2D} and σ_0 are the two free parameters used for the fitting of the curve. The fit of the data points to the mathematical model perfectly coincides with the experimental curve obtained, indicating the appropriateness of the mathematical model used. However, in order to extract the 2D Young's modulus (E_{2D}) of the membrane, the force-deflection curve must reach the cubic regime. A logarithmic graph(base 10) of the force-deflection data is depicted in fig 4c. The graph shows that, at high loads, our indentation measurements reaches the cubic regime, which indicates that the value extracted is the true 2D Young's modulus (E_{2D}).

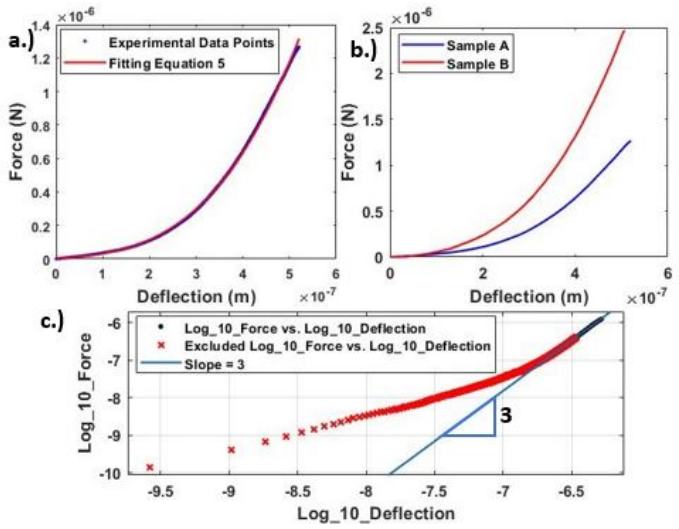

Fig. 4. a.) Indentation curve fitting to equation 5 of one of the membranes, b.) Indentation curve comparing the two samples, c.) $\log_{10}$ Force vs $\log_{10}$ Deflection plot indicating that the curve has reached the cubic regime.

The above mentioned mathematical model (eq 5) was used to estimate the pretension (σ_0) and the 2D Young's modulus (E_{2D}) of the membranes. Thirty-four membranes of sample A and forty membranes of sample B have been measured in total. Statistical analysis was performed for the values extracted from the different membranes. Histogram plots (fig 5) for the values of E_{2D} and σ_0 were obtained for both the samples. The solid red line in fig 5 is the distribution fit associated with the derived values. A normal distribution fit was used in the case of E_{2D}, and a Weibull distribution fit was used in the case of σ_0. The Weibull distribution was used to make sure the distribution fit does not provide negative values of σ_0. Based on the statistical analysis, for sample A, E_{2D} was found to be 140.42 $\pm$ 44.52 N/m and σ_0 was 0.119 $\pm$ 0.049 N/m. Meanwhile, for sample B, E_{2D} was found to be 393.34 $\pm$ 145.12 N/m and σ_0 was 0.203 $\pm$ 0.069 N/m. In both cases, there existed no correlation between E_{2D} and σ_0. To understand the obtained values in simpler terms, a comparative force-deflection plot (4b) was obtained between two membranes, one from each sample. The plot shows that the membrane from sample A deflects more than the membrane from sample B for the same quantity of force applied by the cantilever, which implies that sample A is a softer membrane when compared to sample B.

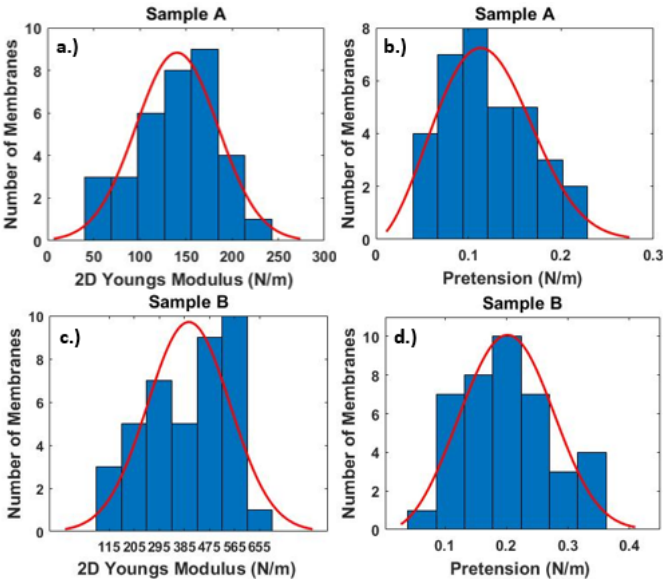

Fig. 5. Histogram of a.) sample A 2D Young's modulus (E_{2D}), b.) sample A pretension (σ_0), c.) sample B 2D Young's modulus (E_{2D}), d.) sample B pretension (σ_0)

Considering the values extracted for sample A, which is a monolayer CVD graphene, the values of E_{2D} fall short of the expected value of the pristine graphene (342 N/m)[2]. As mentioned earlier, Nicholl et al.[14] also observed the softening of the CVD graphene membranes. They showed that static wrinkles present in the membranes are the primary cause. In addition, the AFM images of sample A (fig:3a) also show that the membranes are not perfectly flat or pristine and that they possess out-of-plane crumples. The values of E_{2D} obtained for sample A are in agreement with the values extracted by Nicholl et al.[14] in their work. The formation of these crumples or static wrinkles could be due to the uneven stress distribution experienced by the CVD graphene during the fabrication or transfer of the film[21].

On the other hand, sample B is a monolayer CVD graphene subjected to increased surface pressure by adding 0.1% liquinox. The idea behind this is that a kind of compressive force acts on the graphene flake due to the increased surface pressure, and since the bending rigidity of graphene is very low, the graphene flake gets crumpled from all sides. However, the degree of crumpling is not uniform, so quantifying the amount of crumpling is not easy. Surprisingly, when compared to sample A, the E_{2D} of sample

B is considerably high.

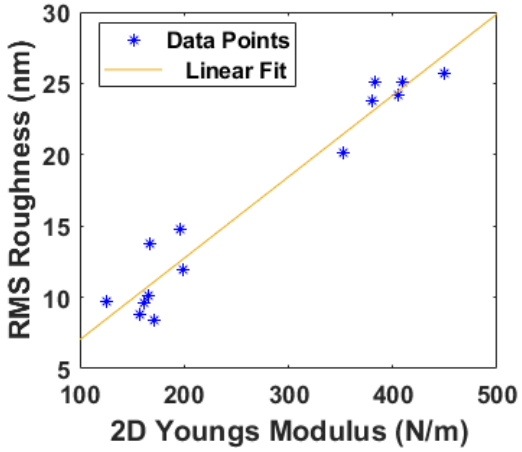

Fig. 6. Plot of 2D Young's modulus (E_{2D}) vs RMS roughness of the membrane

Previous theoretical works[10] show that crumpling of graphene tends to degrade the material and possess less in-plane stiffness. In addition, sample A also follows a similar trend. However, on the contrary, the membranes of sample B show a slight hardening behaviour. In order to comprehend this contradicting result, the degree of crumpling is quantified in terms of the root mean square(RMS) value of the membrane roughness. The RMS roughness of a membrane is obtained from the topography of the membrane cross-section. The waviness of the topography, as shown in fig 3 (c-d), is taken into consideration when estimating the RMS value of the membrane roughness. A plot of E_{2D} vs the RMS roughness of membranes is depicted in fig 6. The plot obtained shows a linear dependence between the RMS roughness and E_{2D}. However, this plot cannot be justified entirely as, for pristine membranes(approximately 0 nm RMS roughness), the plot depicts the membrane to be very soft, which contradicts the findings of Lee et al.[2] and also does not make sense. On the other hand, for non-pristine membranes, the linear dependency between E_{2D} and the amount of crumpling can be justified. In this case, the out-of-plane deformations in the membranes collapse over each other to form folds that are visible in the AFM images (fig:3b). These folds act as localised multi-layer graphene and provide greater resistance (second-order elastic stiffness) to the applied force compared to monolayer graphene. This dependency is also the reason for the large standard deviation obtained for E_{2D} of the membranes.

After the nanoindentation of the heavily crumpled membranes, the membranes are imaged again to understand the deformation of the membrane. The AFM image of one of the membranes after nanoindentation is depicted in fig7b. The topology of the cross-section of the membrane (fig:7c) depicts a sizeable upward plastic deformation around the centre of the membrane. The upward direction of the deformation is observed as the membrane gets attached to the tip of the

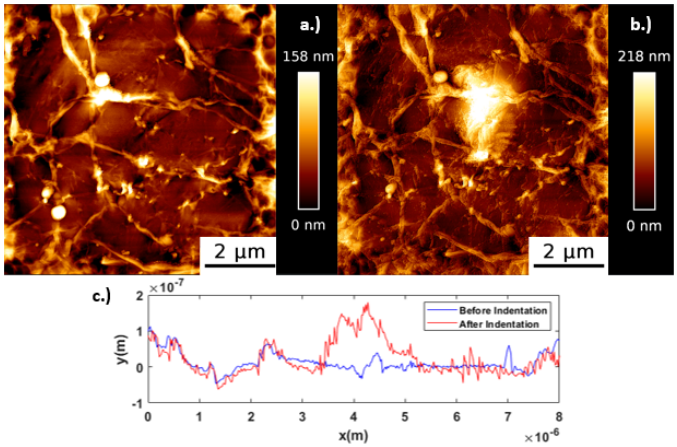

Fig. 7. AFM image of a graphene membrane a.)before and b.)after the nanoindentation measurement, c.) The topology profile of the cross-section showing the upward deformation of the membrane.

cantilever during the retraction of the cantilever to the preset set point, which causes the membrane to be pulled upwards. Interestingly, the hidden area under the folds and crumples in the graphene membrane is opened up at high loads, leading to an increase in the area of the graphene membrane. Since the dimension of the hole is fixed, the membrane slacks in the out-of-plane direction and this slack is seen in the form of the large deformation. In order to support the deformation

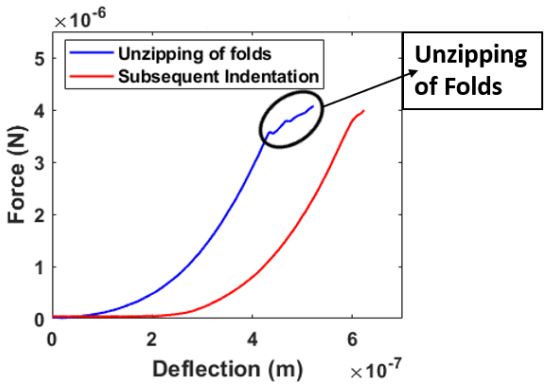

Fig. 8. (Solid Blue line) The force-deflection characteristics depicting the unzipping of the folds and the bubbled region is the instant at which the folds open up, (Solid Red line) The force-deflection characteristics of the subsequent indentation.

of the membrane, the force-deflection characteristics depicting the unzipping of the folds and the subsequent indentation are obtained, as shown in fig 8. The solid blue line depicting the membrane's indentation leading to the opening up of folds shows how the force-deflection curve deviates from the usual trend due to the opening up of folds. During this phenomenon, a sudden increase in the deflection of the membrane is expected, and this increase was observed in the force-deflection curve (fig: 8 bubbled region) of the membrane. The opened up membrane was again indented, and the force-deflection curve (fig: 8 red solid line) depicts the behaviour of the deformed

membrane under loading. The near horizontal behaviour at the start of the indentation clearly shows the presence of slack in the membranes, and as mentioned earlier, the slack formation is due to the opening up of the folds.

IV. Conclusion

AFM imaging and nanoindentation of two sets of samples, Sample (A) - CVD graphene and Sample (B) - heavily crumpled CVD graphene, were performed to study the effects of crumpling on the in-plane stiffness of the graphene membrane. For this purpose, the samples were fabricated using a simple wet transfer method as shown in fig 1. 20μl of 0.1% liquinox was added to the etchant solution to obtain the heavily crumpled sample. The samples were first imaged using the AC mode of the AFM, and these images clearly show the difference between the two sets of samples. Further, these membranes were indented using the AFM in the contact mode, from which the force-deflection characteristics for both set of samples were obtained. The obtained force-deflection curves were fit using the available mathematical model[20], with pretension (σ_0) (N/m) and 2D Young's modulus (E_{2D}) (N/m) as the free parameters.

For sample A, a value of 140.42 $\pm$ 44.52 N/m and 0.119 $\pm$ 0.049 N/m were obtained for E_{2D} and σ_0 respectively. Meanwhile, for sample B, a value of 393.34 $\pm$ 145.12 N/m and 0.203 $\pm$ 0.069 N/m were obtained for E_{2D} and σ_0 respectively. Since sample A is not completely pristine, the values of E_{2D} extracted were justifiable and were in agreement with the previous studies[14]. However, the values of E_{2D} extracted for sample B contradict the general trend. Since thickness was not considered, nothing can be said about the Young's modulus (Pascals) and intrinsic strength of the membrane. The membranes were also imaged after the nanoindentation, which depicted a large plastic deformation in the upward direction around the centre of the membrane. This large deformation was due to the unzipping of the folds present around the centre of the membrane.

To conclude, it can be said that by crumpling the graphene film, the membrane may start to act as multi-layered films and provide greater resistance to deflection, depending on the amount of crumpling present. This resistance is reflected in the increased E_{2D}. In order to understand the actual effect of the crumples, it would be better to open up the existing folds before indenting the membrane or try to extract the Young's modulus and intrinsic strength using another measurement technique.

References

[1] A. A. Balandin, S. Ghosh, W. Bao, I. Calizo, D. Teweldebrhan, F. Miao, and C. N. Lau, "Superior thermal conductivity of single-layer graphene," *Nano Letters*, vol. 8, no. 3, pp. 902–907, mar 2008. [Online]. Available: https://pubs.acs.org/doi/abs/10.1021/nl0731872

[2] C. Lee, X. Wei, J. W. Kysar, and J. Hone, "Measurement of the Elastic Properties and intrinsic Strength of Monolayer Graphene," vol. 321, no. July, pp. 385–389, 2008.

[3] K. Bolotin, K. Sikes, Z. Jiang, M. Klima, G. Fudenberg, J. Hone, P. Kim, and H. Stormer, "Ultrahigh electron mobility in suspended graphene," *Solid State Communications*, vol. 146, no. 9, pp. 351–355, 2008. [Online]. Available: https://www.sciencedirect.com/science/article/pii/S0038109808001178

[4] R. R. Nair, P. Blake, A. N. Grigorenko, K. S. Novoselov, T. J. Booth, T. Stauber, N. M. Peres, and A. K. Geim, "Fine structure constant defines visual transparency of graphene," *Science*, vol. 320, no. 5881, p. 1308, jun 2008. [Online]. Available: https://science.sciencemag.org/content/320/5881/1308https://science.sciencemag.org/content/320/5881/1308.abstract

[5] S. Chatterjee, J. Wang, W. Kuo, N. Tai, C. Salzmann, W. Li, R. Hollertz, F. Nüesch, and B. Chu, "Mechanical reinforcement and thermal conductivity in expanded graphene nanoplatelets reinforced epoxy composites," *Chemical Physics Letters*, vol. 531, pp. 6–10, 2012. [Online]. Available: https://www.sciencedirect.com/science/article/pii/S0009261412001789

[6] M. J. Nine, M. A. Cole, D. N. H. Tran, and D. Losic, "Graphene: a multipurpose material for protective coatings," *J. Mater. Chem. A*, vol. 3, pp. 12 580–12 602, 2015. [Online]. Available: http://dx.doi.org/10.1039/C5TA01010A

[7] B. Zhan, C. Li, J. Yang, G. Jenkins, W. Huang, and X. Dong, "Graphene field-effect transistor and its application for electronic sensing," *Small*, vol. 10, no. 20, pp. 4042–4065, 2014. [Online]. Available: https://onlinelibrary.wiley.com/doi/abs/10.1002/smll.201400463

[8] O. E. Kwon, J.-W. Shin, H. Oh, C. mo Kang, H. Cho, B.-H. Kwon, C.-W. Byun, J.-H. Yang, K. M. Lee, J.-H. Han, N. S. Cho, J. H. Yoon, S. J. Chae, J. S. Park, H. Lee, C.-S. Hwang, J. Moon, and J.-I. Lee, "A prototype active-matrix oled using graphene anode for flexible display application," *Journal of Information Display*, vol. 21, no. 1, pp. 49–56, 2020. [Online]. Available: https://doi.org/10.1080/15980316.2019.1680452

[9] M. Pumera, "Graphene-based nanomaterials for energy storage," *Energy Environ. Sci.*, vol. 4, pp. 668–674, 2011. [Online]. Available: http://dx.doi.org/10.1039/C0EE00295J

[10] S. Deng and V. Berry, "Wrinkled, rippled and crumpled graphene: An overview of formation mechanism, electronic properties, and applications," *Materials Today*, vol. 19, no. 4, pp. 197–212, 2016. [Online]. Available: http://dx.doi.org/10.1016/j.mattod.2015.10.002

[11] F. Banhart, J. Kotakoski, and A. V. Krasheninnikov, "Structural defects in graphene," *ACS Nano*, vol. 5, no. 1, pp. 26–41, 2011.

[12] A. Tapia, R. Peón-Escalante, C. Villanueva, and F. Avilés, "Influence of vacancies on the elastic properties of a graphene sheet," *Computational Materials Science*, vol. 55, pp. 255–262, apr 2012.

[13] S. Lee, "Effect of Intrinsic Ripples on Elasticity of the Graphene Monolayer," *Nanoscale Research Letters*, vol. 10, no. 1, dec 2015. [Online]. Available: /pmc/articles/PMC4621976//pmc/articles/PMC4621976/?report=abstracthttps://www.ncbi.nlm.nih.gov/pmc/articles/PMC4621976/

[14] R. J. Nicholl, H. J. Conley, N. V. Lavrik, I. Vlassiouk, Y. S. Puzyrev, V. P. Sreenivas, S. T. Pantelides, and K. I. Bolotin, "The effect of intrinsic crumpling on the mechanics of free-standing graphene," *Nature Communications*, vol. 6, 2015.

[15] A. Obraztsov, E. Obraztsova, A. Tyurnina, and A. Zolotukhin, "Chemical vapor deposition of thin graphite films of nanometer thickness," *Carbon*, vol. 45, no. 10, pp. 2017–2021, 2007. [Online]. Available: https://www.sciencedirect.com/science/article/pii/S0008622307002965

[16] V. E. Calado, G. F. Schneider, A. M. M. G. Theulings, C. Dekker, and L. M. K. Vandersypen, "Formation and control of wrinkles in graphene by the wedging transfer method," *Applied Physics Letters*, vol. 101, no. 10, p. 103116, 2012. [Online]. Available: https://doi.org/10.1063/1.4751982

[17] M. Lanza, Y. Wang, A. Bayerl, T. Gao, M. Porti, M. Nafria, H. Liang, G. Jing, Z. Liu, Y. Zhang, Y. Tong, and H. Duan, "Tuning graphene morphology by substrate towards wrinkle-free devices: Experiment and simulation," *Journal of Applied Physics*, vol. 113, no. 10, p. 104301, 2013. [Online]. Available: https://doi.org/10.1063/1.4794521

[18] M. F. C. Z. e. a. Bao, W., "Controlled ripple texturing of suspended graphene and ultrathin graphite membranes," *Nature Nanotech*, vol. 4, p. 562–566, 2009. [Online]. Available: https://doi.org/10.1038/nnano.2009.191

[19] A. Agius Anastasi, "Nanoindentation of graphene membranes using atomic force microscopy and molecular dynamics simulations," 2021.

[20] W. Wang, S. Li, J. Min, C. Yi, Y. Zhan, and M. Li, "Nanoindentation experiments for single-layer rectangular graphene films: a molecular dynamics study," *Nanoscale research letters*, vol. 9, no. 1, pp. 1–8, 2014.
[21] L.-P. Ma, W. Ren, and H.-M. Cheng, "Transfer methods of graphene from metal substrates: A review," *Small Methods*, vol. 3, no. 7, p. 1900049, 2019.

6

Conclusion

The main objective of this research was to determine how the mechanics of the graphene membrane change in the presence of out-of-plane deformations in the form of crumples. The literature review, done to understand the present level of research in the field of graphene mechanics, shows the practical limitations present during the membranes' testing. The major limitation was the presence of structural or surface imperfections in the obtained graphene membrane. Literature shows that researchers have been able to study the effects of these imperfections theoretically. In addition, experimental validation of the effect of point defects[23] and line defects[61] have also been reported. However, the effect of static wrinkles or crumples on the mechanics of graphene are yet to be experimentally obtained.

In order to study the effect of crumples, two types of membranes were fabricated, one was a flat CVD graphene membrane, and the other was a heavily crumpled CVD graphene membrane. In both cases, the films were transferred onto Si/SiO_2 substrates with square through holes. The heavily crumpled sample was obtained by adding liquinox to the etchant solution. Liquinox was essentially used to reduce the surface tension of the etchant solution and, in turn, compress the graphene film. The atomic force microscope (AFM) was used to probe the membranes. The AFM was first used in the tapping mode to image the membranes and then used in the contact mode to perform the nanoindentation of these membranes. The existing mathematical model[70] was then used to extract the pretension (σ_0) and 2D Young's modulus (E_{2D}) values from the force-deflection characteristics of the membrane.

In the case of flat membranes, a value of 140.42 ± 44.52 N/m and 0.119 ± 0.049 N/m were obtained for E_{2D} and σ_0 respectively. Since the obtained graphene membranes were not perfectly pristine and possessed some crumples, the obtained values were way lower than those reported in the literature. Meanwhile, for the heavily crumpled sample, a value of 393.34 ± 145.12 N/m and 0.203 ± 0.069 N/m were obtained for E_{2D} and σ_0 respectively. Based on the values extracted and the large standard deviation, we can say that the 2D Young's modulus of the membrane is dependent on the amount of crumpling present in the membrane. The heavy crumpled membrane's deformation after the nanoindentation was also looked into by again imaging the sample using the AFM. The opening up of the folds around the centre of the membrane could be seen from the images.

This research has provided an idea of how the mechanical constants, σ_0 and E_{2D}, vary in the presence of crumples. The work also shows how the crumples react to the force applied during the nanoindentation measurements. These results can be further used while realising future applications based on crumpled graphene films. However, mechanical constants like Young's modulus and intrinsic strength of the crumpled graphene are yet to be studied, affecting the progress in the possible applications.

7

Recommendations

This chapter suggests the various improvements that can be made to this work and the different methods that could be followed to possibly obtain a better understanding of the results.

Fabrication of Crumpled Graphene

The possible limitation of the technique used in this research is the use of the liquid phase shrinking of the graphene film. There is always a possibility of residual aqueous films or droplets being trapped between the sample and the target substrates. A substrate with through holes was used solely to avoid this phenomenon. In addition, substrates with through holes possess their own limitations. Other testing methods like electrostatic gating and bulge test cannot be performed using these substrates.

One of the possible alternatives to deal with this issue could be the use of pre-stretched elastomer films onto which pristine graphene can be transferred, and then when the elastomer is relaxed, the graphene film gets crumpled[58]. The other possibility is the CVD of graphene on pre-trenched copper foils[59].

Measurement Methodology

The thickness of the graphene samples are not considered in this study as obtaining the effective thickness of the membrane was not possible using the AFM due to the possibility of an aqueous film being trapped between the substrate and the graphene sample. Since the thickness is not obtained, mechanical constants like Young's modulus and Intrinsic strength could not be obtained.

One of the recommendations is to strain the membrane to open up the crumples before indenting the membrane with the AFM cantilever tip. The membranes can be strained by electrostatic gating, pressurising the membranes, or biaxial stretching of the film by using MEMS or NEMS devices. By doing so, the effect of the strain-induced on the mechanics of the crumpled graphene can also be studied.

Other Recommendations

Since the crumpling of graphene in this work is not in a controlled manner, obtaining control over the amount of crumpling could be an interesting study. In addition, by gaining control over the crumpling developed, the applications of the crumpled membranes can be better realised.

Appendix

A

JPK AFM Setup

In this section, some of the key steps done during the AFM imaging and nanoindentation are explained. The AFM used is the JPK NanoWizard 4 NanoScience AFM, and the images and curves are processed using the JPK SPM Data Processing Software. The imaging was performed using using a silicon cantilever (NCLR, Nanoworld) coated with aluminium (detector side). The nominal resonance frequency of the cantilever is around 170 kHz and the spring constant is around 30 N/m. The dimension of the cantilever used are as follows, thickness is 7 μm, length is 225 μm and width is 38 μm. The image of the entire JPK AFM setup is shown in fig A.1.

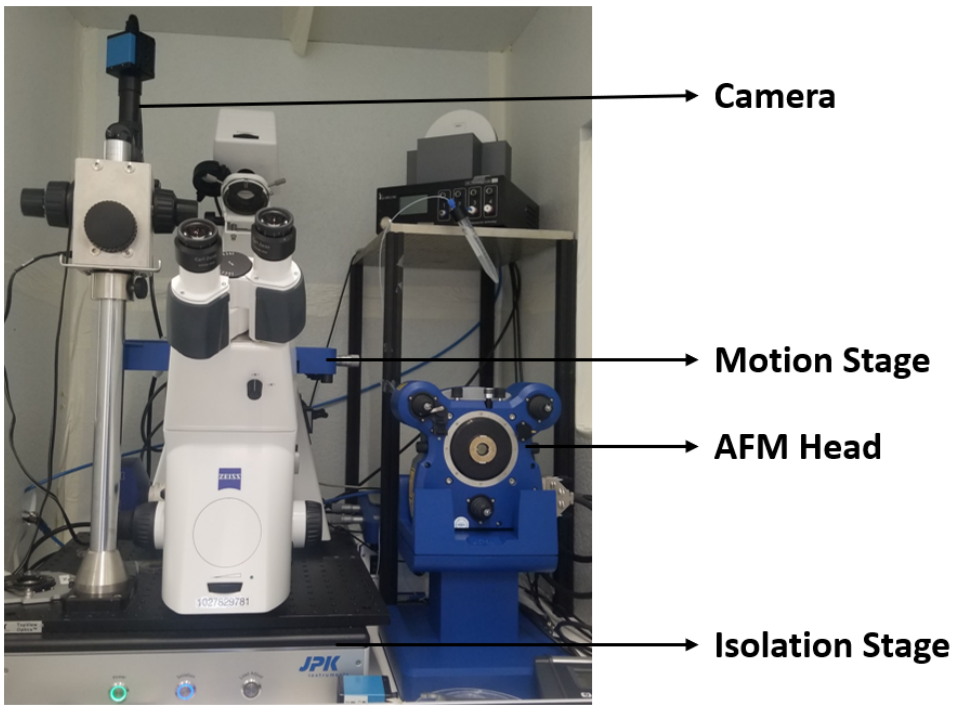

Figure A.1: Image of the entire JPK AFM setup

Some of the important steps that are done during the measurement are as follows,

Step 1: Alignment of the laser on the AFM cantilever and alignment of the photo-diode to make sure the laser spot is in the center.

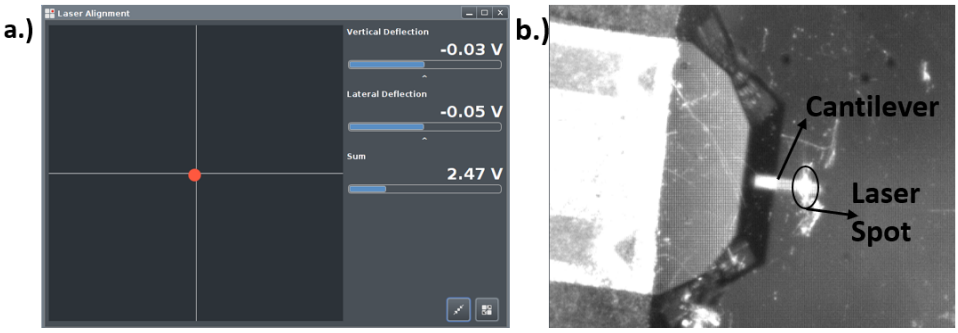

Figure A.2: a.) Alignment of the laser spot on the photodiode, b.) Alignment of the laser spot on the cantilever

Step 2: Calibration of the AFM cantilever response. The specifications of the cantilever are entered and after calibration we obtain the sensitivity, spring constant and resonance frequency of the cantilever.

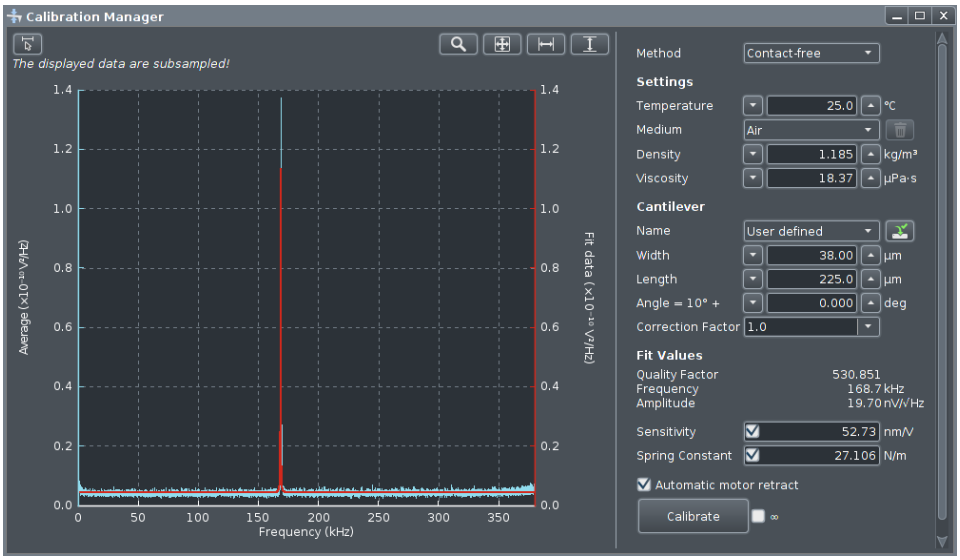

Figure A.3: Image showing the calibration of the AFM cantilever

Depending on the mode of usage of the AFM the subsequent steps are done,

AC/Tapping Mode Imaging

Step 3: Setting the initial feedback. This is mainly done to set the drive frequency and amplitude of the cantilever. It is important that the drive frequency is set close to the resonance frequency of the cantilever.

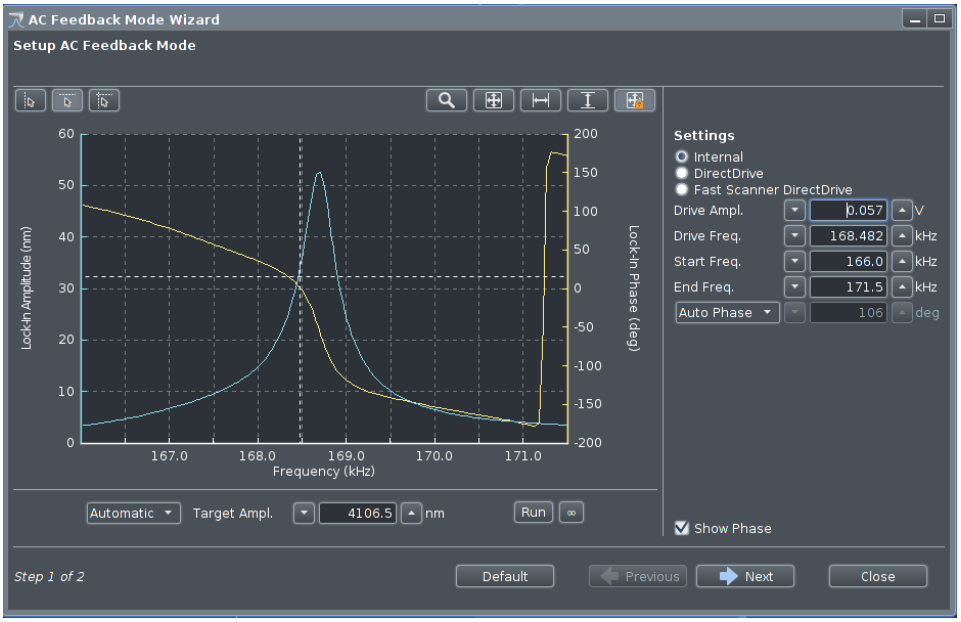

Figure A.4: Setting of the initial feedback of the scanning mode

Step 4: If the feedback is not correctly set, the trace and retrace scans wouldn't coincide properly in the oscilloscope. The feedback can then be altered while the imaging is taking place, with the controls as in fig A.5. The scan area and the rate at which the imaging is taking place can be altered as well.

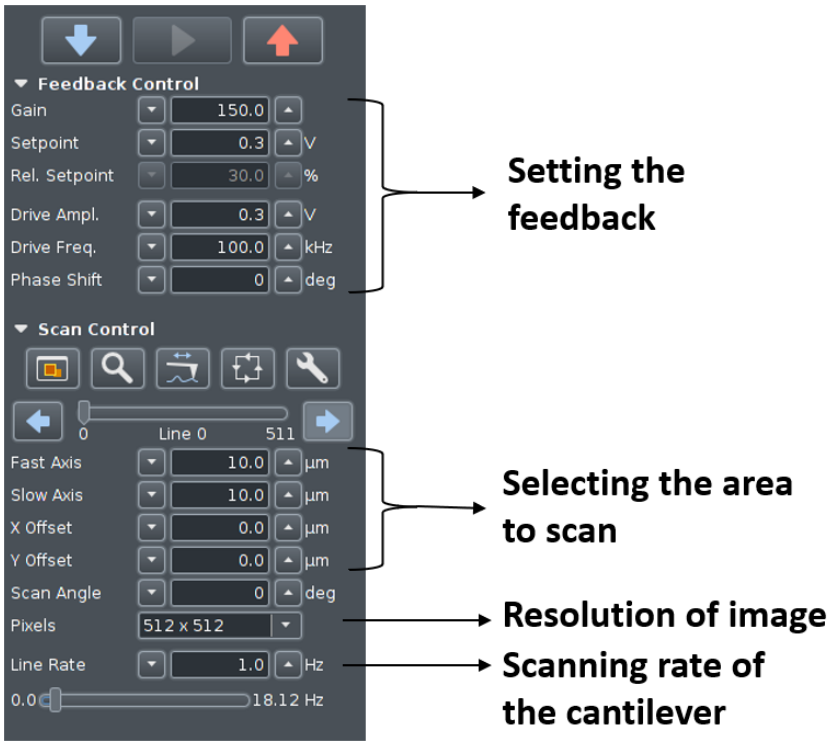

Figure A.5: Options to change the feedback of the controller, scan area and scan rate.

Contact Mode Indentation

Step 3: Setting the initial parameters for the indentation of the samples. Some of the important parameters are setting the feedback controller, number of times the indentation takes place at the same point, the rate of indentation, z-length which is the length of approach, etc.

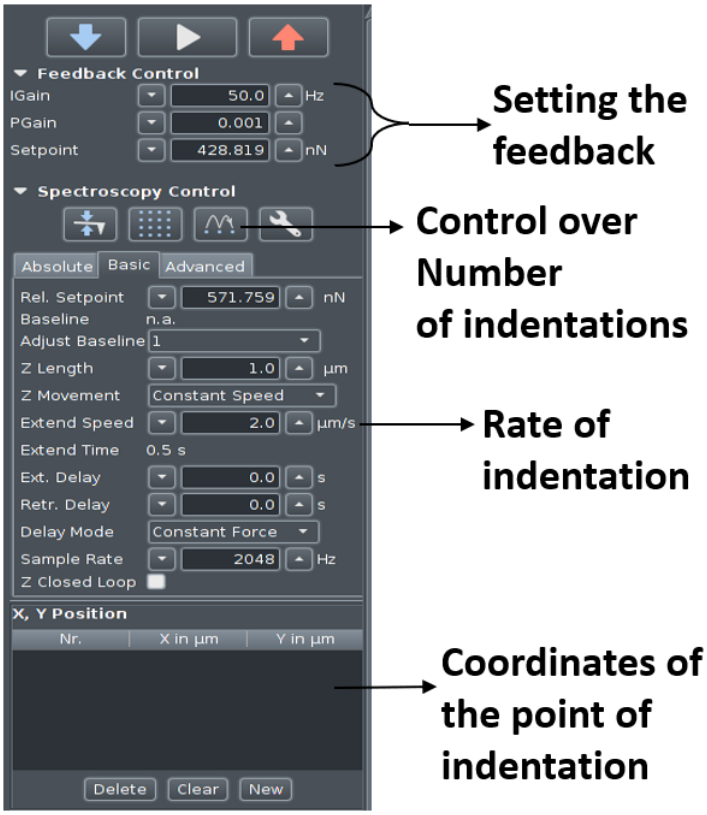

Figure A.6: Options to change the parameters involved in the indentation of samples

B

Processing the Force-Deflection Characteristics

This section deals with the post processing steps that are done to obtain the Force-Deflection data points from the curve obtained from the AFM.

Once, the force-deflection curve is opened in the JPK data processing software, it would look like the fig B.1. The data that we extract from this would be a completely unprocessed data which cannot be used in the mathematical model. In this window, as you can see, we can format the curve that is present like changing parameter in the axes or limits of the axes and so on.

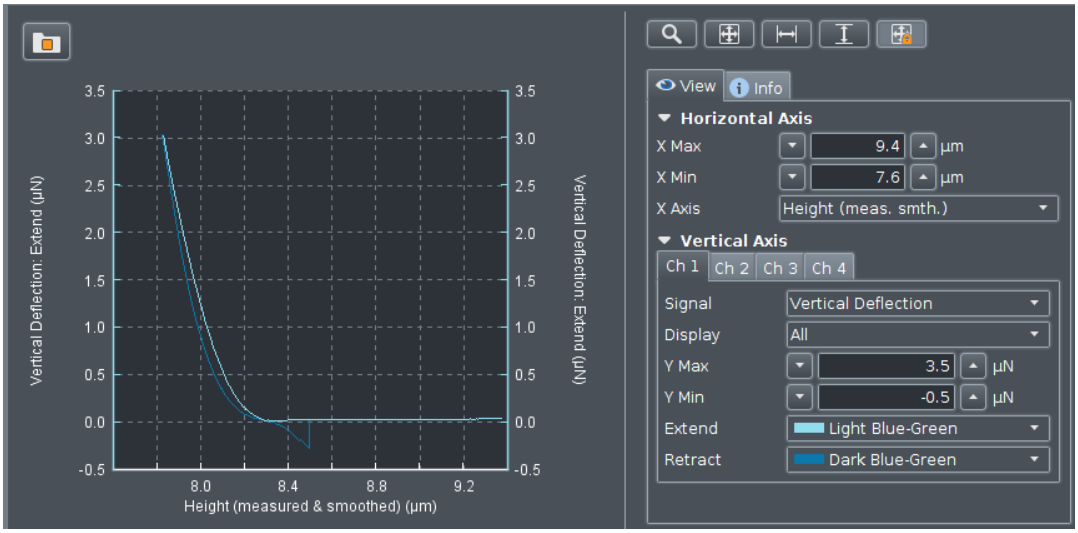

Figure B.1: Unprocessed Force-Deflection Curve

A number of operations need to be done using the software to obtain the true Force-Deflection curve of the membrane and the operations are as follows (B.2),
Step 1: Checking the calibration of the cantilever. The values of the sensitivity and spring constant of the cantilever can also be changed if necessary.
Step 2: Smoothing the data curve.
Step 3: Automatically subtract the baseline. This operation helps in setting the y-offset and obtaining the true force experienced by the membrane.
Step 4: Automatically set the x-offset. This operation helps in obtaining the origin of the force-deflection curve and also find the contact point in the graph.

Step 5: Fit slope and height of the curve.
Step 6: Shifting of origin. The origin of the curve can be manually shifted using this operation.
Step 7: Correcting the height/deflection of the membrane by accounting for the bending of the cantilever.

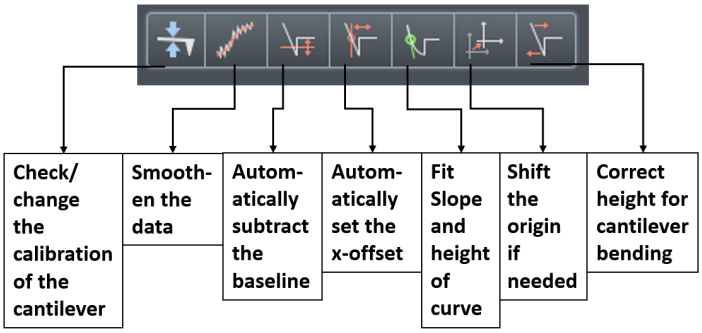

Figure B.2: Operations to obtain true force-deflection curve

The force-deflection curve after these set of operations are performed on the curve is shown in fig B.3. The data points are the exported from this in the form of text file and used in a MATLAB code to extract the mechanical constants.

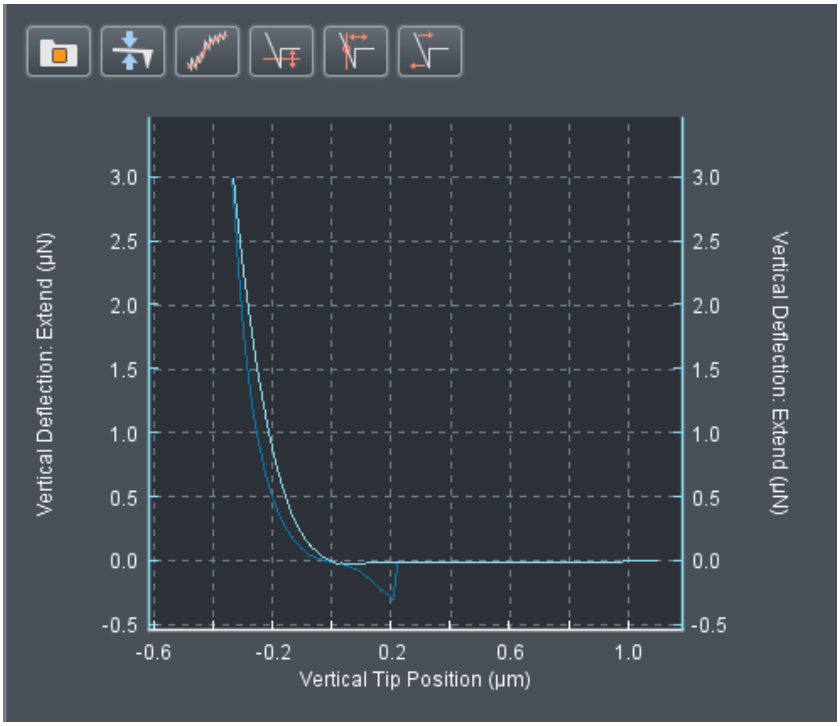

Figure B.3: Corrected Force-Deflection Curve

C

Curve Fitting

The section is basically the MATLAB code which was used to extract the values of pretension (σ_0) and 2D Young's modulus (E_{2D}) of the membranes from their force-deflection characteristics.

```
close all
clear all
clc
load('Data_Set.mat') % The data points of the Force-Deflection
    characteristics
%% Define the constants in the Mathematical model

l = 8e-6; % The side of the square membrane (m)
req= sqrt(l^2/pi); %Calculating the equivalent radius (m)
g = 0.165; % Poisson's ration of graphite in basal plane
q = 1/(1.05-0.15*g-0.16*g^2); % Non-dimensional Quantity

%% Curve Fitting of one of the sets of data

F = Force';
inden = -Def'; % Redefining the data of force and indentation

f = @(k,x) pi*k(1).*x+((q^3)/(req^2))*k(2).*(x).^3; % Mathematical model
    interms of free parameters pretension (k1) and 2D Young's modulus (k2) and
     x is the deflection


K = fminsearch(@(k) norm(F - f(k,inden)), rand(2,1)); % Curve fitting
delta = linspace(min(inden), max(inden));

%% Plotting the Data set along with the curve fit

figure(1)
plot(inden, F, '-b','LineWidth',1)
hold on
plot(delta, f(K,delta), '-r','LineWidth',1.5)
hold off
ylabel('Force (N)'); xlabel('Deflection (m)');
legend('Data set','Fit to Mathematical Model')
```

D

Data Set

This section of the appendix has the link to the data sets that was obtained during the course of the thesis.
https://docs.google.com/spreadsheets/d/1_AoPm2Se_K_vceSt1z4uSDCWPebiztQpWWrtdTyec40/edit?usp=sharing

Bibliography

[1] K. S. Novoselov, A. K. Geim, S. V. Morozov, D. Jiang, Y. Zhang, S. V. Dubonos, I. V. Grigorieva, and A. A. Firsov, "Electric field effect in atomically thin carbon films," Science, vol. 306, no. 5696, pp. 666–669, 2004.

[2] C. Lee, X. Wei, J. W. Kysar, and J. Hone, "Measurement of the Elastic Properties and intrinsic Strength of Monolayer Graphene," vol. 321, no. July, pp. 385–389, 2008.

[3] S. Deng and V. Berry, "Wrinkled, rippled and crumpled graphene: An overview of formation mechanism, electronic properties, and applications," Materials Today, vol. 19, no. 4, pp. 197–212, 2016.

[4] F. Banhart, J. Kotakoski, and A. V. Krasheninnikov, "Structural defects in graphene," ACS Nano, vol. 5, no. 1, pp. 26–41, 2011.

[5] K. S. Kim, Y. Zhao, H. Jang, S. Y. Lee, J. M. Kim, K. S. Kim, J. H. Ahn, P. Kim, J. Y. Choi, and B. H. Hong, "Large-scale pattern growth of graphene films for stretchable transparent electrodes," Nature, vol. 457, pp. 706–710, feb 2009.

[6] K. Bolotin, K. Sikes, Z. Jiang, M. Klima, G. Fudenberg, J. Hone, P. Kim, and H. Stormer, "Ultrahigh electron mobility in suspended graphene," Solid State Communications, vol. 146, no. 9, pp. 351–355, 2008.

[7] L. Zhao, R. He, K. T. Rim, T. Schiros, K. S. Kim, H. Zhou, C. Gutiérrez, S. P. Chockalingam, C. J. Arguello, L. Pálová, D. Nordlund, M. S. Hybertsen, D. R. Reichman, T. F. Heinz, P. Kim, A. Pinczuk, G. W. Flynn, and A. N. Pasupathy, "Visualizing individual nitrogen dopants in monolayer graphene," Science, vol. 333, no. 6045, pp. 999–1003, 2011.

[8] R. R. Nair, P. Blake, A. N. Grigorenko, K. S. Novoselov, T. J. Booth, T. Stauber, N. M. Peres, and A. K. Geim, "Fine structure constant defines visual transparency of graphene," Science, vol. 320, p. 1308, jun 2008.

[9] A. A. Balandin, S. Ghosh, W. Bao, I. Calizo, D. Teweldebrhan, F. Miao, and C. N. Lau, "Superior thermal conductivity of single-layer graphene," Nano Letters, vol. 8, pp. 902–907, mar 2008.

[10] A. A. Balandin, "Thermal properties of graphene and nanostructured carbon materials," jul 2011.

[11] N. Mounet and N. Marzari, "First-principles determination of the structural, vibrational and thermodynamic properties of diamond, graphite, and derivatives," Phys. Rev. B, vol. 71, p. 205214, May 2005.

[12] W. Gao and R. Huang, "Thermomechanics of monolayer graphene: Rippling, thermal expansion and elasticity," Journal of the Mechanics and Physics of Solids, vol. 66, pp. 42–58, may 2014.

[13] D. Vella and B. Davidovitch, "Indentation metrology of clamped, ultra-thin elastic sheets," Soft Matter, vol. 13, no. 11, pp. 2264–2278, 2017.

[14] R. Nicklow, N. Wakabayashi, and H. G. Smith, "Lattice dynamics of pyrolytic graphite," Physical Review B, vol. 5, pp. 4951–4962, jun 1972.

[15] N. Lindahl, D. Midtvedt, J. Svensson, O. A. Nerushev, N. Lindvall, A. Isacsson, and E. E. B. Campbell, "Determination of the Bending Rigidity of Graphene via Electrostatic Actuation of Buckled Membranes," 2012.

[16] M. K. Blees, A. W. Barnard, P. A. Rose, S. P. Roberts, K. L. McGill, P. Y. Huang, A. R. Ruyack, J. W. Kevek, B. Kobrin, D. A. Muller, and P. L. McEuen, "Graphene kirigami," Nature, vol. 524, pp. 204–207, aug 2015.

[17] P. Zhang, L. Ma, F. Fan, Z. Zeng, C. Peng, P. E. Loya, Z. Liu, Y. Gong, J. Zhang, X. Zhang, P. M. Ajayan, T. Zhu, and J. Lou, "Fracture toughness of graphene," Nature Communications, vol. 5, pp. 1–7, 2014.

[18] A. J. Stone and D. J. Wales, "Theoretical studies of icosahedral C60 and some related species," Chemical Physics Letters, vol. 128, pp. 501–503, aug 1986.

[19] J. C. Meyer, C. Kisielowski, R. Erni, M. D. Rossell, M. F. Crommie, and A. Zettl, "Direct imaging of lattice atoms and topological defects in graphene membranes," Nano Letters, vol. 8, pp. 3582–3586, nov 2008.

[20] M. C. Wang, C. Yan, L. Ma, N. Hu, and M. W. Chen, "Effect of defects on fracture strength of graphene sheets," Computational Materials Science, vol. 54, pp. 236–239, mar 2012.

[21] Y. Fu, T. Ragab, and C. Basaran, "The effect of Stone-Wales defects on the mechanical behavior of graphene nano-ribbons," Computational Materials Science, vol. 124, pp. 142–150, nov 2016.

[22] A. Tapia, R. Peón-Escalante, C. Villanueva, and F. Avilés, "Influence of vacancies on the elastic properties of a graphene sheet," Computational Materials Science, vol. 55, pp. 255–262, apr 2012.

[23] G. López-Polín, C. Gómez-Navarro, V. Parente, F. Guinea, M. I. Katsnelson, F. Pérez-Murano, and J. Gómez-Herrero, "Increasing the elastic modulus of graphene by controlled defect creation," Nature Physics, vol. 11, no. 1, pp. 26–31, 2015.

[24] B. W. Jeong, J. Ihm, and G. D. Lee, "Stability of dislocation defect with two pentagon-heptagon pairs in graphene," Physical Review B - Condensed Matter and Materials Physics, vol. 78, p. 165403, oct 2008.

[25] J. Lahiri, Y. Lin, P. Bozkurt, I. I. Oleynik, and M. Batzill, "An extended defect in graphene as a metallic wire," Nature Nanotechnology, vol. 5, pp. 326–329, mar 2010.

[26] A. Fasolino, J. H. Los, and M. I. Katsnelson, "Intrinsic ripples in graphene," Nature Materials, vol. 6, no. 11, pp. 858–861, 2007.

[27] P. Xu, M. Neek-Amal, S. D. Barber, J. K. Schoelz, M. L. Ackerman, P. M. Thibado, A. Sadeghi, and F. M. Peeters, "Unusual ultra-low-frequency fluctuations in freestanding graphene," Nature Communications, vol. 5, pp. 1–7, apr 2014.

[28] H. S. Seung and D. R. Nelson, "Defects in flexible membranes with crystalline order," Physical Review A, vol. 38, pp. 1005–1018, jul 1988.

[29] W. Gao and R. Huang, "Thermomechanics of monolayer graphene: Rippling, thermal expansion and elasticity," Journal of the Mechanics and Physics of Solids, vol. 66, pp. 42–58, may 2014.

[30] S. Lee, "Effect of Intrinsic Ripples on Elasticity of the Graphene Monolayer," Nanoscale Research Letters, vol. 10, dec 2015.

[31] K. V. Zakharchenko, M. I. Katsnelson, and A. Fasolino, "Finite temperature lattice properties of graphene beyond the quasiharmonic approximation," Physical Review Letters, vol. 102, p. 046808, jan 2009.

[32] R. J. Nicholl, H. J. Conley, N. V. Lavrik, I. Vlassiouk, Y. S. Puzyrev, V. P. Sreenivas, S. T. Pantelides, and K. I. Bolotin, "The effect of intrinsic crumpling on the mechanics of free-standing graphene," Nature Communications, vol. 6, 2015.

[33] A. N. Obraztsov, E. A. Obraztsova, A. V. Tyurnina, and A. A. Zolotukhin, "Chemical vapor deposition of thin graphite films of nanometer thickness," Carbon, vol. 45, pp. 2017–2021, sep 2007.

[34] V. E. Calado, G. F. Schneider, A. M. M. G. Theulings, C. Dekker, and L. M. K. Vandersypen, "Formation and control of wrinkles in graphene by the wedging transfer method," Applied Physics Letters, vol. 101, p. 103116, sep 2012.

[35] K. Min and N. R. Aluru, "Mechanical properties of graphene under shear deformation," Applied Physics Letters, vol. 98, p. 013113, jan 2011.

[36] H. Qin, Y. Sun, J. Z. Liu, and Y. Liu, "Mechanical properties of wrinkled graphene generated by topological defects," Carbon, vol. 108, pp. 204–214, nov 2016.

[37] Y. Zhong, Z. Zhen, and H. Zhu, "Graphene: Fundamental research and potential applications," FlatChem, vol. 4, pp. 20–32, 2017.

[38] J. Chen, M. Duan, and G. Chen, "Continuous mechanical exfoliation of graphene sheets via three-roll mill," J. Mater. Chem., vol. 22, pp. 19625–19628, 2012.

[39] N. V. L. M. e. a. Hernandez, Y., "High-yield production of graphene by liquid-phase exfoliation of graphite," Nature Nanotech, vol. 3, p. 563–568, 2008.

[40] K. S. Suslick and D. J. Flannigan, "Inside a collapsing bubble: Sonoluminescence and the conditions during cavitation," Annual Review of Physical Chemistry, vol. 59, no. 1, pp. 659–683, 2008. PMID: 18393682.

[41] B. Nanzai, K. Okitsu, N. Takenaka, H. Bandow, N. Tajima, and Y. Maeda, "Effect of reaction vessel diameter on sonochemical efficiency and cavitation dynamics," Ultrasonics Sonochemistry, vol. 16, no. 1, pp. 163–168, 2009.

[42] G. Kalita and M. Tanemura, "Fundamentals of chemical vapor deposited graphene and emerging applications," in Graphene Materials (G. Z. Kyzas and A. C. Mitropoulos, eds.), ch. 3, Rijeka: IntechOpen, 2017.

[43] B. Lee, W. Chu, and W. Li, "Effects of Process Parameters on Graphene Growth Via Low-Pressure Chemical Vapor Deposition," Journal of Micro and Nano-Manufacturing, vol. 8, 10 2020. 031005.

[44] W. Ren and H.-m. Cheng, "Transfer Methods of Graphene from Metal Substrates : A Review,"

[45] A. Reina, H. Son, L. Jiao, B. Fan, M. S. Dresselhaus, Z. Liu, and J. Kong, "Transferring and identification of single- and few-layer graphene on arbitrary substrates," The Journal of Physical Chemistry C, vol. 112, no. 46, pp. 17741–17744, 2008.

[46] X. Li, Y. Zhu, W. Cai, M. Borysiak, B. Han, D. Chen, R. D. Piner, L. Colombo, and R. S. Ruoff, "Transfer of large-area graphene films for high-performance transparent conductive electrodes," Nano Letters, vol. 9, no. 12, pp. 4359–4363, 2009. PMID: 19845330.

[47] X. Liang, B. A. Sperling, I. Calizo, G. Cheng, C. A. Hacker, Q. Zhang, Y. Obeng, K. Yan, H. Peng, Q. Li, X. Zhu, H. Yuan, A. R. Hight Walker, Z. Liu, L.-m. Peng, and C. A. Richter, "Toward clean and crackless transfer of graphene," ACS Nano, vol. 5, no. 11, pp. 9144–9153, 2011. PMID: 21999646.

[48] H. H. Kim, S. K. Lee, S. G. Lee, E. Lee, and K. Cho, "Wetting-assisted crack- and wrinkle-free transfer of wafer-scale graphene onto arbitrary substrates over a wide range of surface energies," Advanced Functional Materials, vol. 26, no. 13, pp. 2070–2077, 2016.

[49] W. Regan, N. Alem, B. Alemán, B. Geng, Girit, L. Maserati, F. Wang, M. Crommie, and A. Zettl, "A direct transfer of layer-area graphene," Applied Physics Letters, vol. 96, no. 11, p. 113102, 2010.

[50] B. Wang, M. Huang, L. Tao, S. H. Lee, A.-R. Jang, B.-W. Li, H. S. Shin, D. Akinwande, and R. S. Ruoff, "Support-free transfer of ultrasmooth graphene films facilitated by self-assembled monolayers for electronic devices and patterns," ACS Nano, vol. 10, no. 1, pp. 1404–1410, 2016. PMID: 26701198.

[51] W.-H. Lin, T.-H. Chen, J.-K. Chang, J.-I. Taur, Y.-Y. Lo, W.-L. Lee, C.-S. Chang, W.-B. Su, and C.-I. Wu, "A direct and polymer-free method for transferring graphene grown by chemical vapor deposition to any substrate," ACS Nano, vol. 8, no. 2, pp. 1784–1791, 2014. PMID: 24471977.

[52] J. Chan, A. Venugopal, A. Pirkle, S. McDonnell, D. Hinojos, C. W. Magnuson, R. S. Ruoff, L. Colombo, R. M. Wallace, and E. M. Vogel, "Reducing extrinsic performance-limiting factors in graphene grown by chemical vapor deposition," ACS Nano, vol. 6, no. 4, pp. 3224–3229, 2012. PMID: 22390298.

[53] D. J. Z. D. e. a. Zhang, Z., "Rosin-enabled ultraclean and damage-free transfer of graphene for large-area flexible organic light-emitting diodes.," Nat Commun, vol. 8, no. 14560, 2017.

[54] G. J. Fechine, I. Martin-Fernandez, G. Yiapanis, R. Bentini, E. S. Kulkarni, R. V. Bof de Oliveira, X. Hu, I. Yarovsky, A. H. Castro Neto, and B. Özyilmaz, "Direct dry transfer of chemical vapor deposition graphene to polymeric substrates," Carbon, vol. 83, pp. 224–231, 2015.

[55] R. W. X. H. e. a. Gao, L., "Repeated growth and bubbling transfer of graphene with millimetre-size single-crystal grains using platinum.," Nat Commun, vol. 3, no. 699, 2012.

[56] S. Koh, Y. Saito, H. Kodama, and A. Sawabe, "Epitaxial growth and electrochemical transfer of graphene on ir(111)/-al2o3(0001) substrates," Applied Physics Letters, vol. 109, no. 2, p. 023105, 2016.

[57] W. Bao, F. Miao, Z. Chen, H. Zhang, W. Jang, C. Dames, and C. N. Lau, "Controlled ripple texturing of suspended graphene and ultrathin graphite membranes," Nature Nanotechnology, vol. 4, pp. 562–566, jul 2009.

[58] J. Zang, S. Ryu, N. Pugno, Q. Wang, Q. Tu, M. J. Buehler, and X. Zhao, "Multifunctionality and control of the crumpling and unfolding of large-area graphene," Nature Materials, vol. 12, no. 4, pp. 321–325, 2013.

[59] K. K. Bai, Y. Zhou, H. Zheng, L. Meng, H. Peng, Z. Liu, J. C. Nie, and L. He, "Creating one-dimensional nanoscale periodic ripples in a continuous mosaic graphene monolayer," Physical Review Letters, vol. 113, no. 8, pp. 1–5, 2014.

[60] W. Chen, X. Gui, B. Liang, M. Liu, Z. Lin, Y. Zhu, and Z. Tang, "Controllable Fabrication of Large-Area Wrinkled Graphene on a Solution Surface," ACS Applied Materials and Interfaces, vol. 8, no. 17, pp. 10977–10984, 2016.

[61] P. Y. Huang, C. S. Ruiz-Vargas, A. M. Van Der Zande, W. S. Whitney, M. P. Levendorf, J. W. Kevek, S. Garg, J. S. Alden, C. J. Hustedt, Y. Zhu, J. Park, P. L. McEuen, and D. A. Muller, "Grains and grain boundaries in single-layer graphene atomic patchwork quilts," Nature, vol. 469, pp. 389–392, jan 2011.

[62] J. W. Suk, V. Mancevski, Y. Hao, K. M. Liechti, and R. S. Ruoff, "Fracture of polycrystalline graphene membranes by in situ nanoindentation in a scanning electron microscope," physica status solidi (RRL) - Rapid Research Letters, vol. 9, pp. 564–569, oct 2015.

[63] K. Cao, S. Feng, Y. Han, L. Gao, T. Hue Ly, Z. Xu, and Y. Lu, "Elastic straining of free-standing monolayer graphene," Nature Communications, vol. 11, no. 1, pp. 1–7, 2020.

[64] H. H. Pérez Garza, E. W. Kievit, G. F. Schneider, and U. Staufer, "Controlled, reversible, and non-destructive generation of uniaxial extreme strains (>10%) in graphene," Nano Letters, vol. 14, no. 7, pp. 4107–4113, 2014.

[65] K. K. Al-Quraishi, Q. He, W. Kauppila, M. Wang, and Y. Yang, "Mechanical testing of two-dimensional materials: a brief review," International Journal of Smart and Nano Materials, vol. 11, no. 3, pp. 1–40, 2020.

[66] G. López-Polín, M. Jaafar, F. Guinea, R. Roldán, C. Gómez-Navarro, and J. Gómez-Herrero, "The influence of strain on the elastic constants of graphene," Carbon, vol. 124, pp. 42–48, 2017.

[67] Q. Y. Lin, G. Jing, Y. B. Zhou, Y. F. Wang, J. Meng, Y. Q. Bie, D. P. Yu, and Z. M. Liao, "Stretch-induced stiffness enhancement of graphene grown by chemical vapor deposition," ACS Nano, vol. 7, pp. 1171–1177, feb 2013.

[68] Y. Hwangbo, C. K. Lee, S. M. Kim, J. H. Kim, K. S. Kim, B. Jang, H. J. Lee, S. K. Lee, S. S. Kim, J. H. Ahn, and S. M. Lee, "Fracture Characteristics of Monolayer CVD-Graphene," Scientific Reports, vol. 4, pp. 1–9, apr 2014.

[69] C. L. Wong, M. Annamalai, Z. Q. Wang, and M. Palaniapan, "Characterization of nanomechanical graphene drum structures," Journal of Micromechanics and Microengineering, vol. 20, no. 11, 2010.

[70] W. Wang, S. Li, J. Min, C. Yi, Y. Zhan, and M. Li, "Nanoindentation experiments for single-layer rectangular graphene films: a molecular dynamics study," Nanoscale research letters, vol. 9, no. 1, pp. 1–8, 2014.